iScience

CellPress
OPEN ACCESS

Article

Epilepsy gene *prickle* ensures neuropil glial ensheathment through regulating cell adhesion molecules

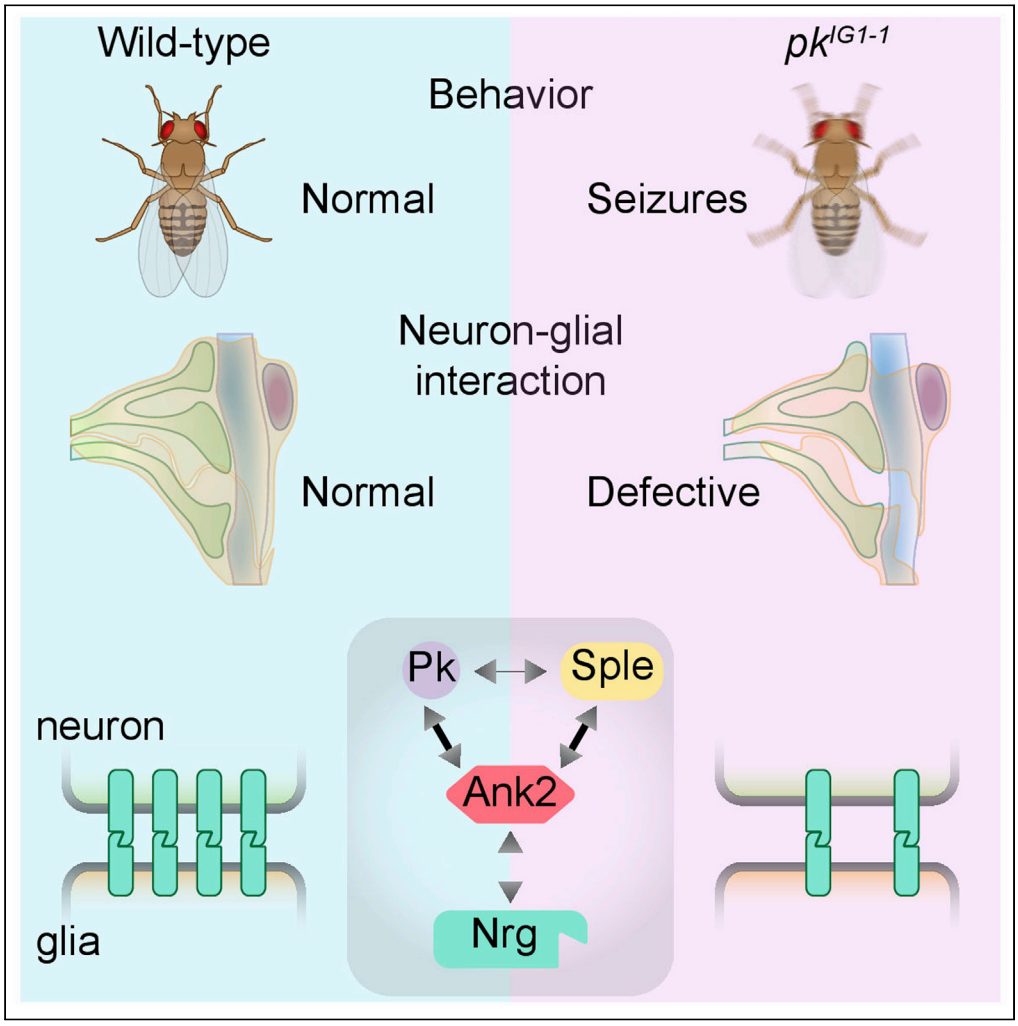

Yanbo Chen, Tong-Tong Liu, Mengxia Niu, Xiaoting Li, Xinwei Wang, Tong Liu, Yan Li

chenyb@ibp.ac.cn (Y.C.)
liyan@ibp.ac.cn (Y.L.)

Highlights

Epileptic *prickle* mutant flies exhibit defective glial wrapping

Expressing Sple isoform in either neurons or glia is sufficient to suppress seizures

prickle is vitally required in neuropil ensheathing glia for suppressing seizures

prickle regulates cell adhesion molecule Neuroglian through Ankyrin 2

Chen et al., iScience *26*, 105731
January 20, 2023
https://doi.org/10.1016/j.isci.2022.105731

iScience

CellPress
OPEN ACCESS

Article

Epilepsy gene *prickle* ensures neuropil glial ensheathment through regulating cell adhesion molecules

Yanbo Chen,[1,4,*] Tong-Tong Liu,[1,2,4] Mengxia Niu,[1] Xiaoting Li,[1,2] Xinwei Wang,[1,2] Tong Liu,[3] and Yan Li[1,2,5,*]

SUMMARY

Human PRICKLE1 gene has been associated with epilepsy. However, the underlying pathogenetic mechanisms remain elusive. Here we report a *Drosophila prickle* mutant pk^{pk1-1} exhibiting strong epileptic seizures and, intriguingly, abnormal glial wrapping. We found that *pk* is required in both neurons and glia, particularly neuropil ensheathing glia (EGN), the fly analog of oligodendrocyte, for protecting the animal from seizures. We further revealed that Pk directly binds to the membrane skeleton binding protein Ankyrin 2 (Ank2), thereby regulating the cell adhesion molecule Neuroglian (Nrg). Such protein interactions also apply to their human homologues. Moreover, *nrg* and *ank2* mutant flies also display seizure phenotypes, and expression of either Nrg or Ank2 rescues the seizures of pk^{pk1-1} flies. Therefore, our findings indicate that Prickle ensures neuron-glial interaction within neuropils through regulating cell adhesion between neurons and ensheathing glia. Dysregulation of this process may represent a conserved pathogenic mechanism underlying PRICKLE1-associated epilepsy.

INTRODUCTION

Epilepsy represents a spectrum of clinically and genetically diverse and intractable neurological disorders characterized by recurrent seizures. Although the etiology of epilepsy is complex, genetic mutations are believed to be a major causal factor. Mutations in human PRICKLE1 were identified in patients from three pedigrees exhibiting progressive myoclonus epilepsy (PME) with ataxia.[1] The accumulating body of evidence of early-onset epilepsy harboring mutations in PRICKLE1 emphasizes its pathogenic effects.[2–5] Mutations in its homolog genes also resulted in epileptic phenotypes in mice, zebrafish and flies, suggesting that the pathogenic mechanisms of PRICKLE1-associated epilepsy are evolutionarily conserved.[1,3,6–9]

prickle (*pk*) was initially identified as a planar cell polarity (PCP) gene in *Drosophila*, and its role in establishing cell polarity has been extensively studied.[10] Two major isoforms of this gene, Prickle (Pk) and Spiny-legs (Sple), named after their phenotypes, has been shown to differently regulate epithelium polarity in various organs, such as wing, notum, leg, and eye.[11,12] In mice, fly and zebrafish, Prickle has also been found to be expressed in the nervous system,[1,3,13] and it participates in various neural developmental processes, including neurite growth, neural migration, and synapse formation and maintenance.[14–17] Notably, Prickle1 was also detected in two types of glia, namely microglia and oligodendrocyte[18]; however, little is known about its function in glial cells.

Glia, which comprise more than half of the population of cells in the human brain, participate in almost all major biological processes of the nervous system.[19] Moreover, their roles have been highlighted in neurological diseases, especially neurodegeneration and epilepsy.[20–22] Microglia serve as immune cells within the CNS, and their proinflammatory function has been suggested to play both pro- and anti-epileptic roles under pathogenic conditions.[23,24] Oligodendrocytes constitute a major component of CNS myelin, which plays essential roles in the maintenance of ionic and transmitter homeostasis.[19] Demyelination is one of the hallmarks of epilepsy in human patients.[22,25–28] Correspondingly, seizures have been found to be common symptoms in demyelinating diseases.[21,29] Moreover, researchers have found a strong association between seizure activity and myelin changes.[30]

[1]Institute of Biophysics, State Key Laboratory of Brain and Cognitive Science, Center for Excellence in Biomacromolecules, Chinese Academy of Sciences, Beijing 100101, China

[2]University of Chinese Academy of Sciences, Beijing 100049, China

[3]International Academic Center of Complex Systems, Advanced Institute of Natural Sciences, Beijing Normal University, Zhuhai 519087, China

[4]These authors contributed equally

[5]Lead contact

*Correspondence: chenyb@ibp.ac.cn (Y.C.), liyan@ibp.ac.cn (Y.L.)

https://doi.org/10.1016/j.isci.2022.105731

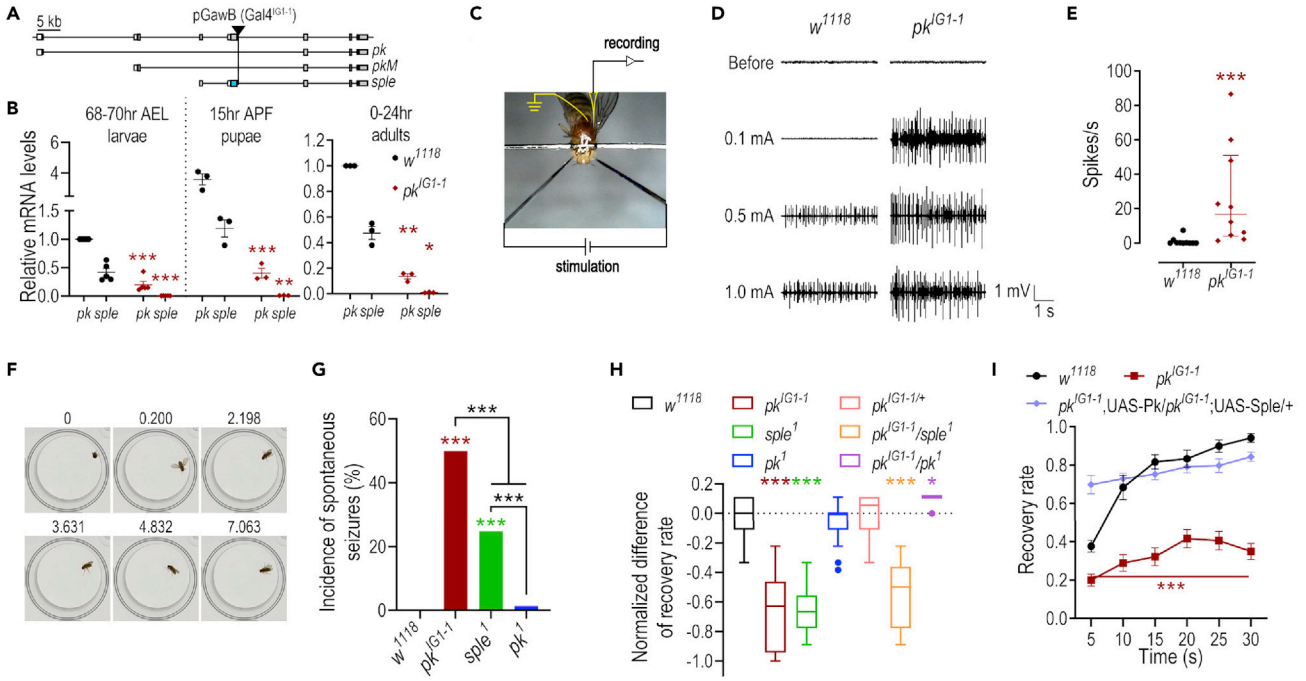

Figure 1. pk^{IG1-1} is a seizure-prone *pk*mutant

(A) Diagram of *Drosophila pk* gene locus. Exons and introns, as well as the insertion site of pGawB element in pk^{IG1-1}mutant are shown on top. Schematic diagrams of three splicing variants are shown below.

(B) Expression levels of *pk* and *sple* transcripts in pk^{IG1-1}mutant and wild-type control w^{1118}. Expression levels of third instar larvae and pupae are normalized to the *pk* levels of w^{1118} larvae, and those of adults are normalized to the *pk* levels of w^{1118} adults. AEL, after egg laying. APF, after pupa formation. two-way ANOVA followed by multiple comparison with Dunnett's correction. n = 3 independent repeats.

(C) Experimental setup of the fly ECS paradigm.

(D) Representative electrographic traces show elicited convulsive spiking activity before and after the delivery of electric stimuli.

(E) Rate of spikes elicited by 0.1 mA stimulation is significantly higher in mutant flies. Mann–Whitney U test. n = 10 flies per group. Median with interquartile range.

(F) A representative spontaneous seizure event is shown by a serial of still images of a free moving pk^{IG1-1} fly. The elapsed time (seconds) is labeled above each image. This fly exhibited convulsive leaping or rolling, and recovered after 7 s.

(G) Incidence of spontaneous seizures during a 5-min period. Fisher's exact test. n> 140 flies per group.

(H) The difference between *pk* mutants and w^{1118} wild-type flies in the recovery rate at 25 s after vortex in the bang-sensitivity assay. One-way ANOVA followed by multiple comparison with Dunnett's correction. Box and whisker plot with Tukey's rule. n> 10 vials for each genotype.

(I) Expressing both Pk and Sple by the Gal4 carried by the P element insertion in pk^{IG1-1} ($Gal4^{IG1-1}$) rescues the seizure defect of pk^{IG1-1} flies in the bang-sensitivity assay. two-way ANOVA followed by multiple comparison with Dunnett's correction. n> 10 vials for each genotype. Mean ± SEM unless otherwise specified. Colored asterisks indicate a significant difference between the group in the corresponding color and w^{1118}. *, p< 0.05; **, p< 0.01; ***, p< 0.001. See also Figure S1.

Here, we identified a fly mutant of *pk*, termed pk^{IG1-1}, which exhibits severe epilepsy-like electrographic and behavioral phenotypes. Further investigation indicated that *pk* is expressed and functions in both neurons and glia to prevent seizures. These findings provided new clues and prompted us to elucidate the molecular and cellular mechanisms underlying the pathogenesis of PRICKLE1-associated epilepsy.

RESULTS

A new *pk* mutant exhibits epilepsy-like seizures

The $Gal4^{IG1-1}$ fly strain was previously reported as a driver line of class I sensory neuron ddaE.[31] As shown in Video S1, we noticed that these flies exhibited uncoordinated leg movement and trembling under normal housing conditions. Using inverse PCR, we localized the insertion site of the transposon to the fourth intron of *pk* gene (Figure 1A). As a result, the expression levels of the two major transcripts, *pk* and *sple*, were both dramatically reduced compared to wild-type (Figure 1B). Thus, we termed this $Gal4^{IG1-1}$ fly strain pk^{IG1-1}mutant.

Recurrent episodes of convulsive discharges of neurons are hallmarks of epilepsy. To test whether this mutant exhibits such epileptic phenotype, we subjected the $pk^{IG1\text{-}1}$mutant flies to the electroconvulsive stimulation (ECS) assay (Figure 1C).[32] As shown in Figure 1D, 0.1 mA current induced few muscular discharges in the dorsal lateral muscle of wild-type control w^{1118} flies. The convulsive muscular discharges were not evident until the stimulation current reached 0.5 mA. However, currents as low as 0.1 mA provoked convulsive discharges in $pk^{IG1\text{-}1}$mutant flies, and the amplitude of the spikes were considerably larger than those recorded from wild-type flies. Moreover, the firing rate following 0.1 mA stimulation was significantly higher in $pk^{IG1\text{-}1}$mutant than the control flies (Figure 1E), indicating that ECS of 0.1 mA evoked strong epileptic activity in the mutant flies.

Spontaneous seizures are one of the typical characteristics of the patients with PRICKLE1 gene mutations.[2] As shown in Video S2, in the absence of external stimulation, $pk^{IG1\text{-}1}$mutant flies occasionally exhibited convulsive leaping or rolling, and sometimes even paralysis. Such unprovoked seizure events typically lasted 2–5 s. We then estimated the incidence of unprovoked seizures by video recording of single free-moving flies in 24-well plates (Figure 1F). As shown in Figure 1G, approximately 50% of $pk^{IG1\text{-}1}$ flies experienced spontaneous seizures, which were not observed in wild-type flies. We compared $pk^{IG1\text{-}1}$ with previously reported *pk* mutants, pk^{1} and $sple^{1}$,[11] the latter of which has been reported to exhibit epilepsy-like phenotypes.[3,6,8] Our data showed that $sple^{1}$mutant also exhibited a significantly higher incidence of spontaneous seizures (24.8%) compared to the wild-type, whereas pk^{1} rarely displayed such defects (1.4%).

We further compared the gene expression levels among these mutants. As shown in Figure S1A, in comparison with wild-type, the mRNA levels of the *pk* transcript were significantly lower in mutants $pk^{IG1\text{-}1}$ and pk^{1} but not $sple^{1}$. For the *sple* transcript, the mRNA levels were significantly lower in all the mutants tested, among which $pk^{IG1\text{-}1}$ showed the lowest expression of *sple*. Accordingly, the *pk:sple* mRNA ratio was highest in $pk^{IG1\text{-}1}$ and lowest in pk^{1} (Figure S1B), and this ratio was correlated with the incidence of spontaneous seizures of these mutantflies (Figure S1C). We further examined the protein levels by Western Blot. Consistently, Pk isoform levels were remarkably lower in $pk^{IG1\text{-}1}$ and pk^{1} flies in comparison with wild-type flies, whereas the Sple isoform was undetectable in $pk^{IG1\text{-}1}$ and $sple^{1}$ mutants (Figure S1D). Collectively, $pk^{IG1\text{-}1}$ represents a new *pk* mutant fly strain, which showed low expression of both isoforms and high incidence of spontaneous seizures.

We next used the bang-sensitivity assay to evaluate the evoked seizure-like behavior in these mutant flies.[32] As shown in Figure 1H, wild-type w^{1118} flies almost completely restored motor control 25 s after vortex treatment (see also Figure S1E). In contrast, the $pk^{IG1\text{-}1}$ flies exhibited paralysis, convulsive wing vibration, as well as flipping after vortex treatment, thus recovered significantly slower than wild-type flies (Video S3). Furthermore, $sple^{1}$, as well as the *trans*-heterozygote $pk^{IG1\text{-}1}/sple^{1}$ flies also recovered significantly slower compared with wild-type. On the contrary, the pk^{1} and $pk^{IG1\text{-}1}/pk^{1}$ flies recovered at rates comparable to the wild-type flies (Figures 1H and S1F). Furthermore, expression of these two isoforms in the homozygous $pk^{IG1\text{-}1}$ background fully rescued the seizure susceptibility of the mutant (Figure 1I). In the control experiments, overexpression of the isoforms did not affect the recovery rate in the bang-sensitivity assay (Figure S1G). Together, these results demonstrated that loss-of-function of *pk* renders $pk^{IG1\text{-}1}$mutant flies susceptible to seizures. Thus, this mutant fly line may serve as a genetic model to study the pathologic mechanisms of PRICKLE1-associated epilepsy.

Pk function in ensheathing glia is required for suppressing seizures

To examine which types of cells in the nervous system are responsible for the generation in *pk* mutant, we expressed Pk or Sple in a $pk^{IG1\text{-}1}$mutant background using a pan-neuronal driver *elav*-LexA and a pan-glial driver *repo*-LexA, respectively. Neuronal expression of Sple partially rescued the bang-sensitivity of the mutant, however, expression of Pk showed no or even exacerbating effects (Figures 2A, 2C, and S2A). Notably, glial expression of Sple achieved similar rescue effects, and expressing Pk failed to rescue the seizure phenotype of $pk^{IG1\text{-}1}$mutant as well (Figures 2B, 2C, and S2A).

Next, we tested whether down-regulating *pk* in neurons or glia is sufficient to induce seizures. Either pan-neuronal or pan-glial knock-down of *pk* (*pk*-KD) resulted in the death of all progenies at the late pupal stage, suggesting that its function is required in both cell types during neural development. As illustrated in Figure 2D, *Drosophila* glia comprise morphologically and genetically distinct subtypes.[33] Therefore, we

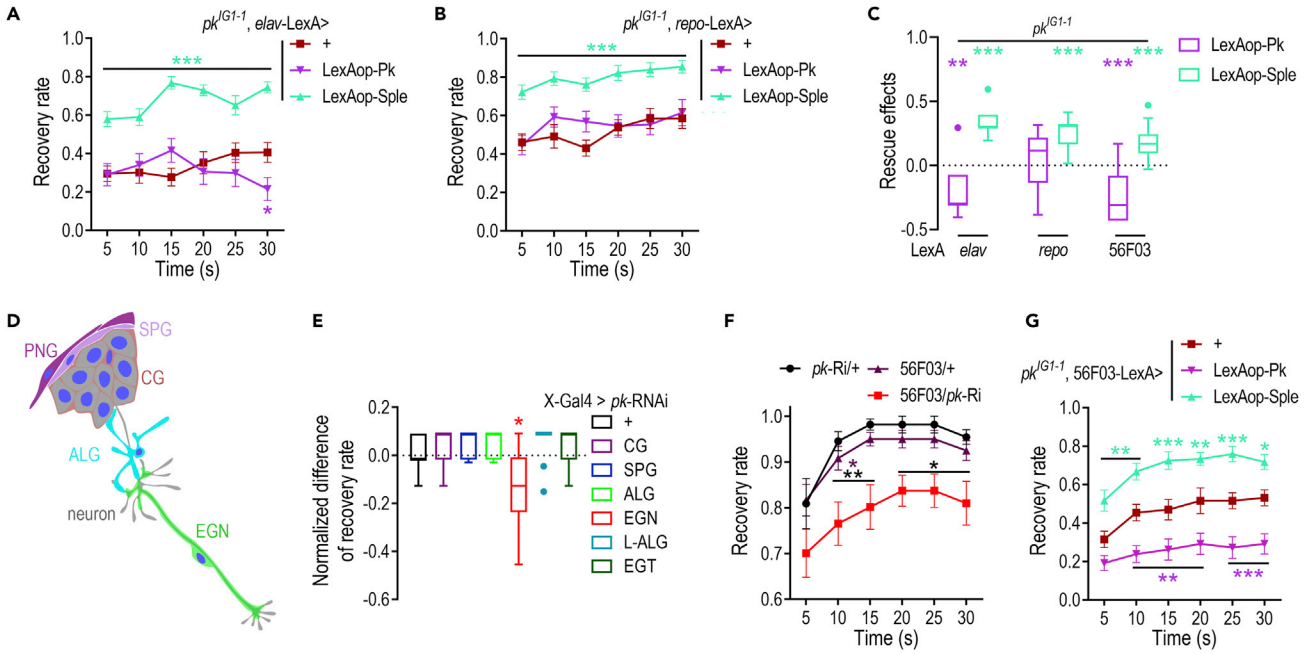

Figure 2. *pk* function is required in both neurons and glia to prevent seizures

(A and B) Pan-neuronal (A) or pan-glial (B) overexpression of Sple, but not Pk suppresses the seizure phenotype of pk^{IG1-1}. two-way ANOVA followed by multiple comparison with Dunnett's correction.

(C) Rescue effects of overexpression of Sple and Pk by various drivers, corresponding to the data at 30 s after vortex in A, B and G panels. One sample *t*-test (H_0: $\mu = 0$).

(D) Cartoon illustration of glial subtypes in fly brain, including perineurial glia (PNG), subperineurial glia (SPG), cortex glia (CG), astrocyte-like glia (ALG), and ensheathing glia neuropil (EGN).

(E) The difference between various glial-KD and the control group (UAS-*pk*-RNAi/+) in the recovery rate at 30 s after vortex in the bang-sensitivity assay. One-way ANOVA followed by multiple comparison with Dunnett's correction. Box and whisker plot with Tukey's rule.

(F) Knock-down of *pk* in EGN (56F03-Gal4) increases seizure susceptibility of flies. Two-way ANOVA followed by multiple comparison with Dunnett's correction.

(G) Overexpression of Sple in EGN suppresses, whereas overexpression of Pk exacerbates the seizure susceptibility of pk^{IG1-1}. two-way ANOVA followed by multiple comparison with Dunnett's correction. n> 10 for each genotype. Colored asterisks indicate significant difference between the group in the corresponding color and the control group. Mean ± SEM unless otherwise specified. *, p< 0.05; **, p< 0.01; ***, p< 0.001.

See also Figure S2.

performed glial subtype specific *pk*-KD. We found that down-regulation of *pk* in perineurial glia (PNG, 85G01-Gal4) resulted in lethality of all pupae similar to that caused by pan-glial KD.

Flies with *pk* knocked-down in other subtypes of glia cells all hatched normally, and these flies were subjected to the bang-sensitivity behavioral assay (Figures 2E and S2B). We found that *pk*-KD in neuropil ensheathing glia (EGN, 56F03-Gal4), but not other subtypes, significantly reduced the recovery rate compared with the control groups (Figures 2E and 2F). Remarkably, EGN-specific expression of Sple significantly ameliorated the seizure phenotype of pk^{IG1-1}mutant to a comparable level of that observed in flies with pan-glia rescue. In contrast, EGN-specific expression of Pk greatly exacerbated the susceptibility to seizures (Figures 2C and 2G). As a control, overexpression of Pk or Sple in either all glia or EGN failed to induce seizures (Figures S2C and S2D).

pk^{IG1-1}mutant shows defective glial morphology

To analyze *pk* expression pattern, we performed immunostaining in both the PNS and the CNS. The $Gal4^{IG1-1}$ is reported to be expressed in the sensory neuron ddaE in the larval PNS.[31] Consistently, we detected the Pk expression in ddaE neurons with an antibody against Pk (Figure 3A). Moreover, the fluorescent signal was also detected in peripheral wrapping glia encompassing the neuron (outlined in Figure 3A). Typically, glial cells wrap the axon, cell body and proximal dendrites of sensory neurons in third instar larvae (Figure 3B). Strikingly, in homozygous pk^{IG1-1}mutant larvae, 33.3% of the ddaE neurons showed incomplete

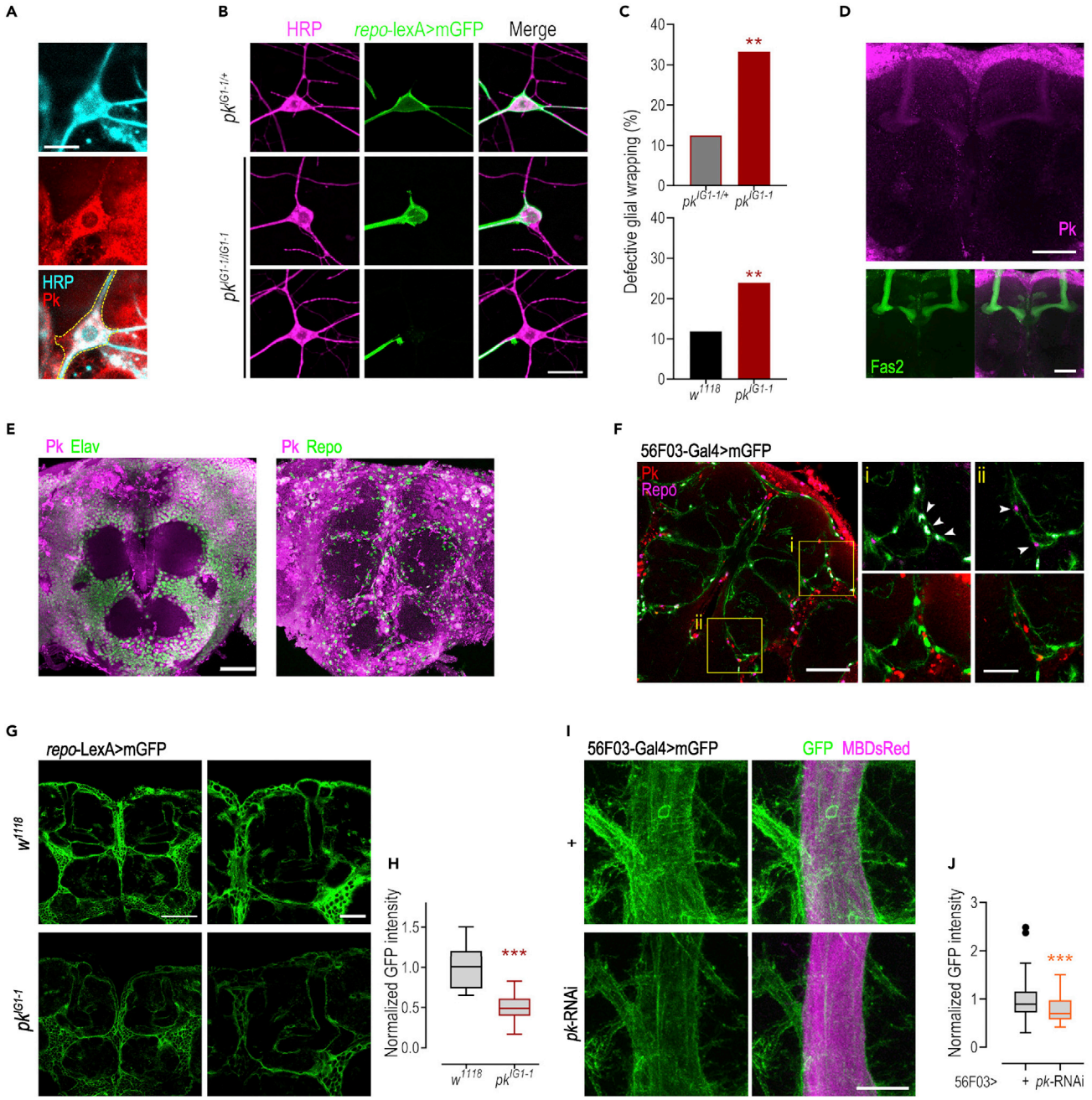

Figure 3. Abnormal glial wrapping in both PNS and CNS of pk^{IG1-1}mutant

(A) Pk antibody-labeled an area (outlined in yellow dash line) encompassed the soma of ddaE neuron. Scale bar: 20 μm

(B) Representative images of ddaE neurons with normal glial wrapping in heterozygous (top row) and defective glial wrapping in homozygous mutant flies (middle and bottom rows). The ddaE neurons were labeled by anti-HRP antibody staining. Glial cells were visualized by mGFP under a glial driver, *repo*-LexA. In the middle row, the cell body was partially stripped of glial sheath, whereas in the bottom row, the entire cell body was bare without glial sheath. Scale bar: 20 μm

(C) The percentage of neurons showing glial wrapping defects is significantly higher in homozygous than in heterozygous pk^{IG1-1}mutant flies (top, n > 60 neurons per group) and higher than in wild-type flies (bottom, n > 160 neurons per group). Fisher's exact test.

(D) Immunostaining with Pk antibody show the expression of Pk in adult brains, particularly enriched in the MB. Fas2 immunofluorescent signals highlight the MB lobes. Scale bar: 50 μm

(E) Confocal images of adult fly brain stained with Pk antibody and neuronal (Elav, left) or glial (Repo, right) markers show that Pk is widely expressed in both neurons and glia. Scale bar: 50 μm

Figure 3. *Continued*

(F) Pk immunostaining signals are found in EGN (labeled by 56F03-Gal4>mGFP and Repo staining). Square ROIs (i and ii) are enlarged, and white arrowheads indicate glial nuclei. Scale bar: left, 50 μm; middle and right, 20 μm

(G) The mGFP signal of CNS glia is weaker in $pk^{IG1\text{-}1}$mutant, compared to that in wild-type. Representative images of brains (left) and the MB lobes (right). Scale bar: left: 50 μm; right: 20 μm

(H) The glial mGFP signal was significantly lower in the mutant flies surrounding the MB lobes. Student's *t* test. n = 10 per group. Box and whisker plot with Tukey's rule.

(I and J) Expression of an RNAi against *pk* (*pk*-KD) in EGN results in reduced glial mGFP signal surrounding the MB peduncle marked by MBDsRed. The Mann Whitney test, n = 50 for each genotype. Box and whisker plot with Tukey's rule. *, p< 0.05; **, p< 0.01; ***, p< 0.001.

See also Figures S3 and S4.

glial wrapping, which was significantly higher than the rate found in either heterozygous $pk^{IG1\text{-}1/+}$ larvae (12.5%, Figures 3B and 3C) or wild-type larvae (11.9%, Figures 3C and S3A). The glial wrapping defects were also observed in $sple^{1}$mutant at a higher rate than control flies (Figures S3B and S3C), suggesting that glial defect is a common phenotype of *pk* mutants.

We next examined the expression pattern of *pk* in the brain. $pk^{IG1\text{-}1}$ carries a copy of Gal4 in *pk* gene (Figure 1A), thus this Gal4 largely represents the expression pattern of *pk*. Driven by this Gal4, both membrane and nuclear localized GFP (mGFP and nlsGFP, respectively) labeled a large number of cells in the adult brain (Figures 3D, S4A, and S4B). In particular, the mGFP signal highlighted a central brain structure, the α/β lobe of the mushroom body (MB, Figure S4C). Consistently, immunostaining signal of Pk was widely detected in the brain with an enrichment in the MB α/β lobe (Figure 3D), in agreement with a previous report.[34]

To determine in which cell type Pk is expressed, we performed co-immunostaining experiments. The results showed that Pk^{+} cells were co-stained with either Elav or Repo, indicating that Pk is expressed in both neurons and glia (Figure 3E). As described above, knock-down of *pk* in PNG and EGN resulted in mortality and seizures, respectively. In agreement, Pk immunostaining signal was detected in these two subtypes of glia (Figures 3F, S4D, and S4E). Notably, we observed Pk^{+} EGN adjacent to the MB (Figure 3Fi), suggesting that Pk may function in both MB neurons and surrounding EGN. In previous reports, elevating the activity of MB increased the susceptibility to seizures.[35,36] We thus focused on the glial morphology around the MB neuropils.

We expressed mGFP under the control of *repo*-LexA. The GFP signal was most evident on the surface of the brain, as well as the sheaths of the MB neuropils (Figure 3G). Under identical imaging conditions, we observed dramatically lower GFP signal in $pk^{IG1\text{-}1}$ brains compared to wild-type brains (Figure 3G). Using the MBDsRed (an DsRed driven by a mushroom body (MB) promoter sequence) as the reference signal to define the margin of the MB, we quantified the GFP signal on the boundary of MB lobes, which was significantly lower in $pk^{IG1\text{-}1}$mutant than in wild-type (Figure 3H). Furthermore, knocking-down *pk* specifically in EGN also resulted in a significant decrease in the GFP signal encompassing the MB lobes (Figures 3I and 3J). In addition, we found that the volume of MB neuropils was slightly but significantly larger in the mutant compared to that of wild-type (Figures S3D–S3H). Taken together, these results indicate that loss-of-function of *pk* results in morphological defects of glia in both PNS and CNS.

Cell adhesion molecule Nrg180 levels are reduced in $pk^{IG1\text{-}1}$ flies

L1-type cell adhesion molecules (L1-CAMs) play important roles in glial wrapping.[37,38] We thus investigated whether defective glial ensheathment in $pk^{IG1\text{-}1}$mutant is associated with dysregulation of these proteins. Nrg is a member of the *Drosophila* L1-CAM family, and Nrg180 is the longer isoform predominantly expressed in fly nervous system. We first examined protein levels of Nrg180 in ddaE neurons by immunostaining. In $pk^{IG1\text{-}1}$mutant, the fluorescent signal was significantly lower in the soma, dendrite, and axon, particularly the proximal regions, in comparison with those in wild-type (Figures 4A–4E).

We next examined the levels of Nrg180 in the MB of adult brain (Figures S5A and S5B). We found that in wild-type flies, Nrg180 protein was enriched in the middle parts of both the peduncle and vertical lobe regions (Figures 4F–4H). In $pk^{IG1\text{-}1}$mutant flies, the protein levels were significantly lower, and the difference was more prominent in the proximal to middle segment of the peduncle, and in the middle segment of the vertical lobe (Figures 4G and 4H). Furthermore, knock-down of *pk* in EGN also resulted in reduced Nrg180

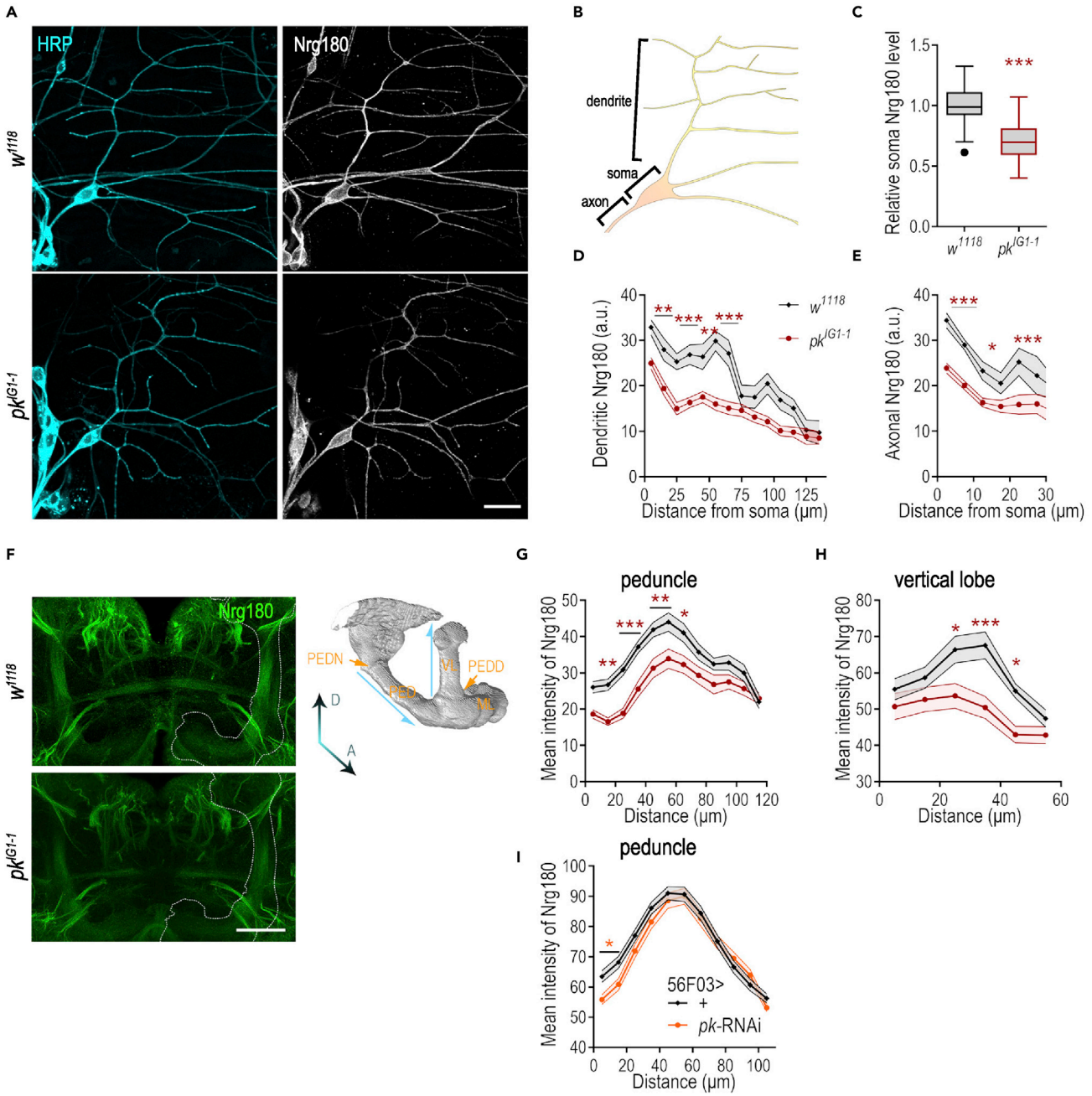

Figure 4. *pk* mutation results in reduced protein levels and abnormal distribution of Nrg180 protein in the nervous system

(A) Larval ddaE neurons co-stained for HRP and Nrg180. Scale bar: 20 μm

(B) Cartoon illustration of dendrites, axon, and the cell soma of a ddaE neuron.

(C) The intensity of Nrg180 staining signal in soma is significantly lower in pk^{IG1-1} than in wild-type larvae. Student's *t*-test. n> 20 for each genotype. Box and whisker plot with Tukey's rule.

(D and E) The Nrg180 protein levels within the initial 70 μm of dendrites (D) and the initial 25 μm of axon (E) in the mutant neurons are significantly lower than those of wild-type neurons. Data are binned every 10 μm for dendrites or 5 μm for axons. Mixed-effects model analysis followed by multiple comparison with Sidak's correction. n> 20 for each genotype.

(F) Representative images of Nrg180 staining signal in wild-type and the mutant brain (left). An illustration of the MB structure with the cyan arrows showing the measurement direction. Scale bar: 50 μm

Figure 4. *Continued*

(G and H) Nrg180 levels are significantly lower in the segment of peduncle 10–70 μm away from the peduncle neck (G) and vertical lobe 20–50 μm away from peduncle divide (H). Data are binned every 10 μm. Mixed-effects model analysis followed by multiple comparison with Sidak's correction, n > 20 for each genotype.

(I) Knock-down of *pk* in EGN results in reduced Nrg180 levels in the MB peduncle. Mixed-effects model analysis followed by multiple comparison with Sidak's correction. n = 50 for each genotype. Mean ± SEM unless otherwise specified. *, p< 0.05; **, p< 0.01; ***, p< 0.001.

See also Figure S5.

levels in the peduncles (Figure 4I). Fas2 is another L1-CAM highly expressed in the MB. In contrast to Nrg180, Fas2 protein levels in $pk^{IG1\text{-}1}$mutant were not different from those in the wild-type control (Figures S5C and S5D). Together, our results showed that loss-of-function of *pk* resulted in reduced protein levels of cell adhesion molecule Nrg, which were more prominent in the initial segment of axons, suggesting that Pk/Sple function is more critically required for Nrg localization in this region.

Ank2 mediates Pk-Nrg180 interaction

We next examined whether Pk/Sple binds Nrg180 using co-immunoprecipitation (co-IP) assay. The results showed that Nrg180 failed to co-precipitate with either Pk or Sple (Figure 5A). Ankyrin represents a group of cytoplasmic proteins that anchor on the membrane skeleton. It has been reported that mammalian Ank3 interacts with L1-CAMs at the nodes of Ranvier.[39,40] Moreover, the *Drosophila* homolog Ank2 was shown to interact with Nrg180.[41] Thus, we tested whether Pk or Sple binds Ank2. We found that a fragment shared by all the isoforms of Ank2 (Ank2-com) co-precipitated with both Pk and Sple (Figure 5B).

We further mapped the binding domains through which Pk/Sple interacts with Ank2. We found that deletion of the LIM-type Zinc fingers (ΔLIM) from Pk-com, the common region of Pk and Sple, abolished the interaction, whereas deletion of Prickle Espinas Testin (PET) domain (ΔPET) or the C-terminal tail (ΔC) retained the binding ability (Figure 5C). For the Ank-com protein fragment, deletion of the Ankyrin-repeat domain (ΔAnk) but not the spectrin-binding domain (ΔSpec) abolished the interaction between Ank2 and Pk (Figure 5D). Together, these findings demonstrated that both Pk and Sple bind to Ank2 through the interaction between LIM domain of Pk/Sple and Ank domain of Ank2. In agreement with previous reports,[41] we showed that the Ank2-com fragment co-precipitated with Nrg180 as well (Figure 5E).

In addition, our co-IP experiments showed an unexpected interaction between Pk and Sple (Figures S6A and S6B). Such interaction was dependent on the common C-terminal fragment of Pk and Sple (Figure S6C). *Drosophila* Pk and Sple show high similarity with their human homolog proteins, prickle-like protein 1 and 2 (Prickle1 and Prickle2, Figure S6D). Consistently, our results showed that human Prickle1 and Prickle2 co-precipitated with the Ankyrin repeat domain of Ank3, the human homolog of *Drosophila* Ank2 (Figures 5F and 5G). Moreover, human Prickle1 also interacted with Prickle2 (Figure S6E). These results indicated that the interactions between Prickle and Ankyrin proteins are evolutionarily conserved (Figure 5H).

Ank2 and Nrg180 act downstream of *pk* in preventing seizures

Next, we examined the protein levels and distribution of Ank2 in larval ddaE neurons. In *Drosophila*, *ank2* encodes 20 isoforms, among which Ank2-XL (extra-large) represents the longest form that is mainly expressed in the nervous system.[42] Similar to Nrg180, we found that Ank2-XL protein levels in the soma, dendrite, and axon of ddaE neurons were significantly lower in $pk^{IG1\text{-}1}$mutant compared to wild-type control (Figure 6). This difference was also more prominent in the proximal dendritic segment (Figure 6C). However, Ank2 levels in the MB of adult brain did not show any significant difference between the mutant and wild-type control (Figures S5E and S5F). In $pk^{IG1\text{-}1}$mutant, Ank2 protein levels were less affected in comparison with Nrg, suggesting that other mechanisms independent of *pk* contribute to stabilizing or recruiting Ank2 in the CNS.

We then tested whether loss of Ank2 or Nrg function also causes defects in glial wrapping. The nrg^{17} fly is a hypomorph *nrg* mutant, which has been shown to exhibit abnormal neurodevelopment, including abnormal axon branching and defective axon extension.[37,43] We found that similar to $pk^{IG1\text{-}1}$ larvae, heterozygous $nrg^{17/+}$ larvae showed defective glial wrapping in more than 20% ddaE neurons examined (Figures 7A and 7B), at a significantly higher rate compared with that of wild-type. Knocking-down *nrg* in glia also impaired glial wrapping of ddaE neurons (Figure S7), in agreement with a previous report.[37] Two mutant alleles of *ank*, $ank2^{M}$ (lacking the Ank2-XL isoform) and $ank2^{f00518}$ (a null allele)[44] are both

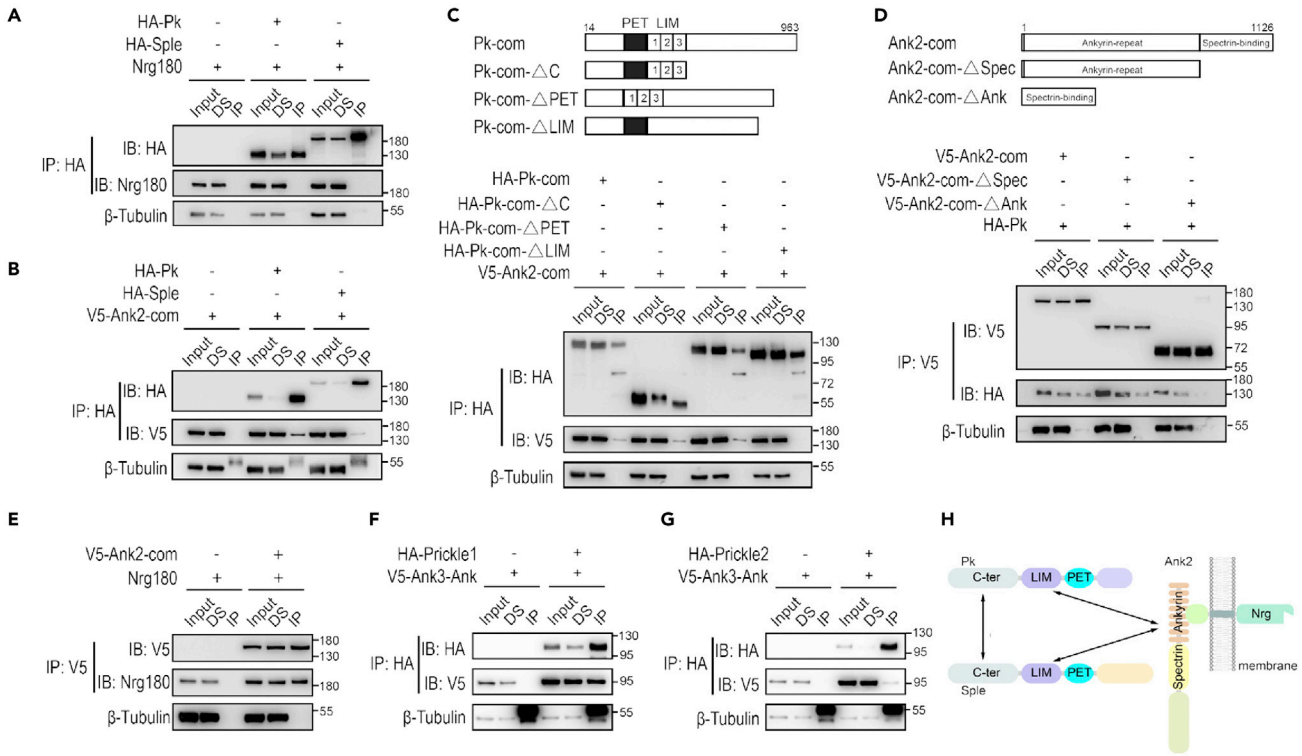

Figure 5. Ank2 mediates interaction of Pk/Sple and Nrg180

(A) Neither Pk nor Sple binds Nrg180.

(B) V5-Ank2-com co-precipitates with Pk and Sple.

(C) Domain diagrams of the common region of *pk* isoforms (Pk-com) with various deletions are shown on the top. HA-tagged Pk-com with LIM domains deleted (HA-Pk-com-ΔLIM) fails to co-precipitate with Ank2-com, whereas other deletions do not affect the binding.

(D) Domain diagrams of the common region of Ank2 isoforms (Ank2-com) with domain deletions are shown on the top. Deletion of Ankyrin repeats (V5-Ank2-com-ΔAnk) abolishes its interaction with Pk, whereas deletion of spectrin binding domain (V5-Ank2-com-ΔSpec) does not affect the binding.

(E) Ank2-com co-precipitates with Nrg180.

(F and G) V5-tagged Ankyrin repeat domain of the human Ank3 protein co-precipitates with both human Prickle1 (F) and Prickle2 (G).

(H) Summary of the biochemical results showing that Ank2 mediates the interaction between Pk/Sple and Nrg. Co-IP experiments were repeated at least three times.

See also Figure S6.

homozygous lethal. We thus examined a *trans*-heterozygous mutant$ank2^{f00518/M}$ for glial wrapping. However, the defective rate of glial wrapping in this mutant was slightly but not significantly higher than that observed in the wild-type control (Figures 7A and 7B). Similarly, the glial wrapping defects were also subtle when we knocked down *ank2* in glia (Figure S7). Given the large number of Ank2 isoforms expressed in the nervous system, we speculate that these isoforms play redundant roles, thus removal of one isoform only results in mild phenotypes.

We next examined whether *nrg* and *ank2* mutant flies display seizures. Using ECS assay, we analyzed convulsive discharges induced by current stimulation in both $nrg^{17/+}$ and $ank2^{f00518/M}$ flies. As shown in Figures 7C and 7D, the firing rate of spikes triggered by 0.1 mA stimulation was higher in both mutant groups compared with the control. When subjected to the bang-sensitive assay, both $nrg^{17/+}$ and $ank2^{f00518/M}$ flies recovered significantly slower than wild-type controls (Figure 7E). Thus, our results demonstrated that mutations in *nrg* and *ank2* genes caused epilepsy-like phenotypes similar to those in pk^{lG1-1} flies.

We then tested whether expressing Nrg180 or Ank2-com could rescue the seizures in pk^{lG1-1}mutant. As shown in Figure 7F, the expression of Nrg fully rescued the bang-sensitivity of pk^{lG1-1}, whereas expression of Ank2 achieved partial rescue. In contrast, overexpression of Fas2 failed to rescue the

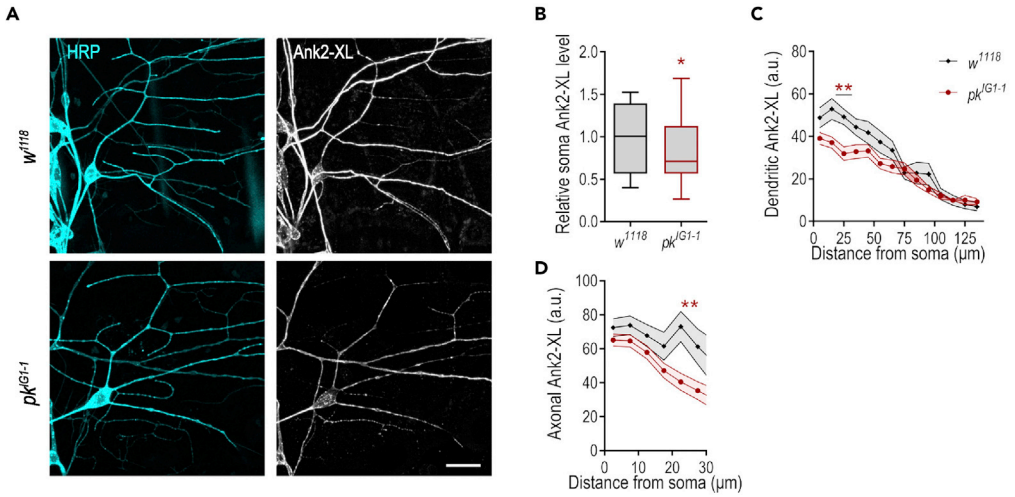

Figure 6. *pk* mutant shows reduced levels and abnormal distribution of Ank2 protein in larval ddaE neurons

(A) ddaE neurons co-stained with HRP and Ank2-XL. Scale bar: 20 μm

(B) The intensity of Ank2-XL immunostaining signals in soma are significantly lower in pk^{IG1-1} than in wild-type larvae. Student's *t*-test. n> 40 neurons. Box and whisker plot with Tukey's rule.

(C and D) The Ank2-XL signals within the 10–30 μm of dendrites (C) and the 20–25 μm of axons (D) in the mutant larvae are significantly lower than those in wild-type. Mixed-effects model analysis followed by multiple comparison with Sidak's correction. n> 20 neurons for each genotype. Mean ± SEM unless otherwise specified. *, p< 0.05; **, p< 0.01.

See also Figure S5.

seizure phenotype. In mammals, Ankyrin and L1-CAMs proteins function in both neurons and glia and play essential roles in the formation of axoglial junction.[45,46] We thus speculated that *pk* also functions in glia by regulating Ank2 and Nrg. To achieve EGN-specific rescue, we generated the pk^{325} allele by the transposase induced hop-out of the Gal4 from pk^{IG1-1} allele. Because of a 325-bp residue, this mutant showed lower expression levels of *pk* and *sple*, which were similar to those in $sple^{1}$mutant (Figures S1A and S1C). On the background of pk^{325}mutant, the expression of Ank2 or Nrg in EGN driven by 56F03-Gal4 rescued the seizure phenotype (Figure 7G). Together, these results indicate that Nrg serves as the key cell adhesion molecule that functions downstream of Pk to mediate the neuron-glial interaction. Moreover, dysfunction of Ank2 and Nrg is involved in the pathogenesis of epilepsy in the pk^{IG1-1}mutant (Figure 7H).

DISCUSSION

In this study, we identified a new *pk* mutant strain, pk^{IG1-1}, that exhibits strong seizure phenotypes. By systematic investigation on this mutant, we found that Pk is expressed in neurons and glia, particularly ensheathing glia, and plays a critical role in neuron-glial interaction via regulating cell adhesion molecules. Thus, our study here provides a new model linking gene mutation, glial defects and pathogenesis.

Our results, together with an earlier report,[34] show that Pk is expressed in the adult CNS, with relatively high expression in the MB. The MB is one of the largest brain structures in adult fly, and the MB neuropils are tightly enwrapped by the EGN.[33] Numerous neurons form dense synaptic connections in the MB and communicate actively to plenty of brain regions, increasing the risk of the propagation of seizure-like convulsive neural activities. In fact, the MB has been implicated in regulating seizure susceptibility.[35,36] Our results showed impaired glial development in the MB neuropils in pk^{IG1-1}mutant. Such defects may lead to dysregulation of synaptic homeostasis and electrical insulation, which could greatly increase the chance of convulsive discharges in the brain and subsequently epileptic seizures.

Drosophila ensheathing glia are categorized into two subtypes, one for the neuropil (EGN), and one for the axon tract (EGT).[33] Our results show that knocking down *pk* in the EGN was sufficient to induce seizures, whereas *pk*-KD in EGT exhibited no effects, indicating that rather than axon tracts, Pk function is critically

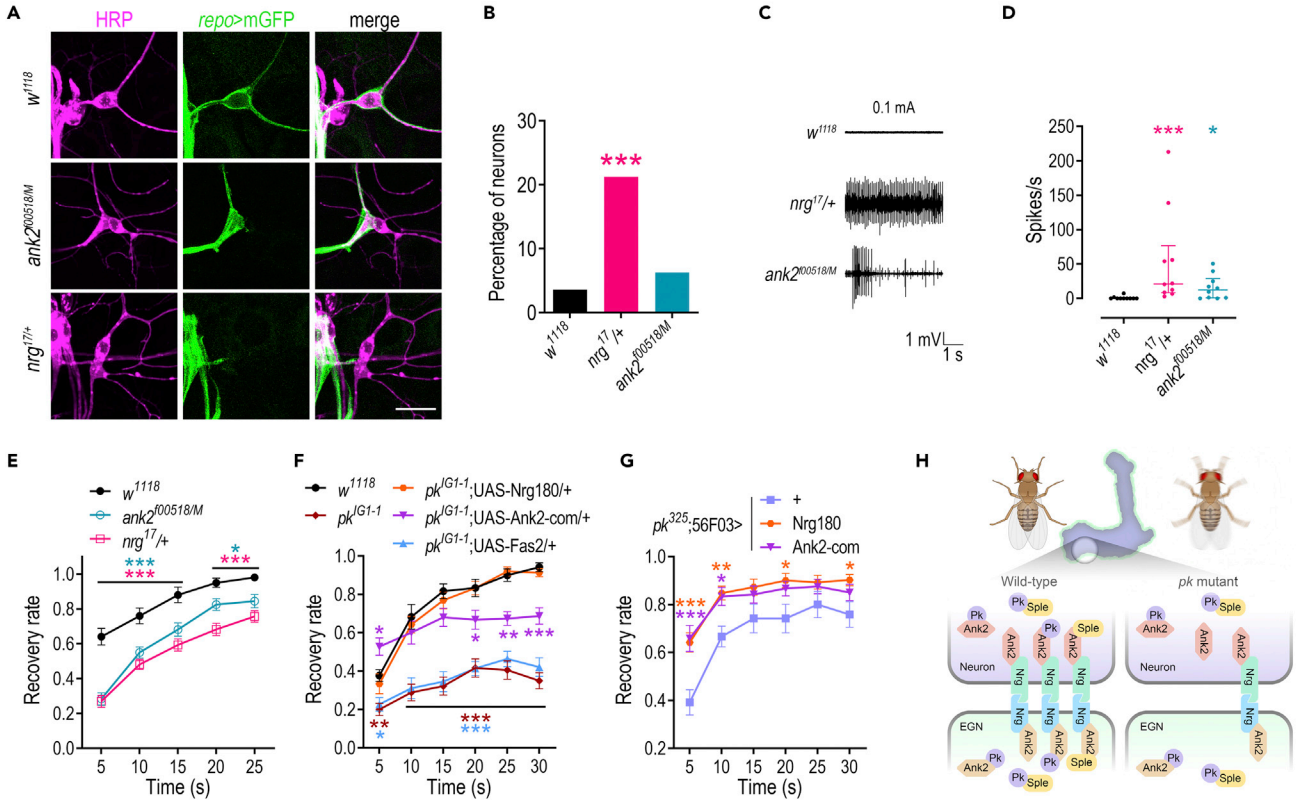

Figure 7. Dysregulation of Ank2 and Nrg180 underlies *pk*-induced seizure

(A) Representative images of ddaE neurons in larvae of wild-type, *trans*-heterozygous mutant of *ank2*, and heterozygous mutant of *nrg*. The ddaE neurons are visualized by HRP staining. Glia are visualized by a *repo*-Gal4>mGFP. Scale bar: 20 μm

(B) The percentage of neurons with defective glial wrapping is significantly higher in $nrg^{17/+}$ larvae than in w^{1118} larvae. Fisher's exact test. n> 20 for each genotype.

(C and D) Elicited by 0.1 mA stimulation, both $ank2^{f00518/M}$ and $nrg^{17/+}$mutant flies exhibit higher firing rate than w^{1118} flies. Kruskal-Wallis test followed by multiple comparison with Dunnett's correction. n = 10 for each genotype. Median with interquartile range.

(E) $ank2^{f00518/M}$ and $nrg^{17/+}$ flies exhibit slower recovery compared with wild-type in bang-sensitive assay. two-way ANOVA followed by multiple comparison with Dunnett's correction.

(F) Overexpression of Ank2-com or Nrg180, but not Fas2, rescues the seizures of pk^{IG1-1} flies. The Gal4 carried by the P element insertion in pk^{IG1-1} ($Gal4^{IG1-1}$) drives the expression. Two-way ANOVA followed by multiple comparisons with Dunnett's correction.

(G) Overexpression of Ank2-com or Nrg180 in EGN rescues the behavioral phenotype of pk^{325}mutant flies. two-way ANOVA followed by multiple comparison with Dunnett's correction. n> 10 for each genotype.

(H) An illustration of *pk* function in regulating neuron-glial interaction in the MB. In wild-type flies, *pk* ensures glial ensheathment through regulating Ank2 and thereby Nrg. Loss-of-function mutation in *pk* results in reduced Nrg protein, and subsequently unstable neuron-glial interaction, which might cause epileptic seizures. Mean ± SEM unless otherwise specified. Colored asterisks indicate significant difference between the group in the corresponding color and the control group. *, p< 0.05; **, p< 0.01; ***, p< 0.001.

See also Figure S7.

required for glial ensheathing of neuropils, which are the sites for extensive synaptic connection. *Drosophila* EG is a structural and functional analog of oligodendrocytes, which constitute myelin in the mammalian brain.[47,48] Intriguingly, an earlier study using knock-in mice reported that Prickle1 is expressed in oligodendrocytes,[18] suggesting that the function of Prickle in glial ensheathment might be evolutionarily conserved. Previous studies suggest that impaired myelin sheath is not only a frequently observed pathological feature of epilepsy, but also actively induces genesis of seizures.[22,27–29,49,50] Based on our findings, we speculate that mutations in human Prickle1 result in dysregulation of glial ensheathment in neuropils and even demyelination, which may contribute to the pathogenesis of PRICKLE1-associated seizures.

Nrg and Fas2 represent two MB-enriched L1-CAM proteins.[38,51] In our study, Nrg but not Fas2 showed decreased protein levels in pk^{IG1-1}mutant, as well as the rescue effect for seizures. Different from Nrg,

Fas2 lacks the ankyrin-binding domain, thus works independently of Ank2.[52] Therefore, our findings highlight Nrg as the Ank-interacting adhesion molecule that functions downstream of *pk*. Human homolog of Nrg, Neurofascin (Nfasc), is also an Ank-interacting L1-CAMs and has been found to play an important role in maintaining neuron-glial interaction.[39,53,54] Notably, recent pedigree studies reported that NFASC is associated with epileptic encephalopathies.[55] Our results showed that human Prickle proteins also bound to human Ank3. Therefore, our findings reveal that the molecular machinery composed of Pk, Ank and Nrg may play an evolutionarily conserved role in regulating neuron-glial interaction, and dysfunction of which greatly increases the seizure susceptibility.

As a core PCP gene, the function of *pk* in establishing epithelial polarity has been extensively studied. Intriguingly, Pk and Sple have been found to play different or even opposite roles.[11,12] In the nervous system, it is also reported that mutants of these two isoforms exhibited divergent seizure susceptibility.[6,8] In agreement with these observations, pan-neural, pan-glial, or EGN-specific expression of Sple, but not Pk, suppressed seizures in $pk^{IG1\text{-}1}$mutant, whereas EGN expression of Pk even aggravated the phenotype. These findings collectively suggest that the Sple isoform plays a protective role against seizure, and the functional divergence of the two isoforms is particularly evident in the EGN.

Pk was previously reported to regulate axonal transport through interacting with Kinesin.[8] Ank3 was found to directly bind Kinesin in regulating the axonal transport of sodium channels in rat neurons.[56] Thus, our findings that the two isoforms of Pk both interacted with Ank2 raise the possibility that Ank2 serves as an adaptor and mediates multiple functions of Pk, such as regulating cell adhesion through Nrg (as shown in this study) and axonal transport through Kinesin.[8,57] Of interest, we identified the interaction between Pk and Sple, as well as between human Prickle1 and Prickle2. We speculate that the mutual interaction among Pk, Sple and Ank2 allows dynamic and multidimensional regulation.

In conclusion, our study uncovers hitherto unidentified aspects of *pk* function in regulating glial ensheathment, and specifies the interacting proteins that are responsible for neuron-glial interaction and the pathogenesis of seizures. On the basis of previous studies and our findings here, we propose that these cellular and molecular mechanisms are evolutionarily conserved. Therefore, our findings provide valuable targets for future studies on the pathogenesis and therapeutic treatment of PRICKLE1-assosciated and NFASC-associated epilepsy.

Limitations of the study

Owing to the lack of specific antibodies against glial Nrg and Ank2, we only examined the protein levels of Ank2-XL and Nrg180, which are both neuronal isoforms. In addition, current Pk antibody was raised against the common region of Pk and Sple, making it impossible to individually determine the protein levels and subcellular distribution of the two isoforms. Further studies with newly generated antibodies will deepen the understanding of the complicated protein interactions within the Pk-Ank2-Nrg molecular machinery. Our current results demonstrate that mutation of *pk* results in impaired glial ensheathment, which potentially affects electrical insulation, ion channel localization, extracellular homeostasis of neurotransmitters and ions, etc. Which of these processes is/are responsible for the generation and propagation of convulsive discharges in the brain and eventually result(s) in epilepsy awaits further elucidation. Future investigation will gain in-depth insights into the regulatory function of *pk* in the nervous system and its roles in the pathogenesis of seizures.

STAR★METHODS

Detailed methods are provided in the online version of this paper and include the following:

- KEY RESOURCES TABLE
- RESOURCE AVAILABILITY
  - Lead contact
  - Materials availability
  - Data and code availability
- EXPERIMENTAL MODEL AND SUBJECT DETAILS
  - Fly strains and constructs
- METHOD DETAILS
  - Behavioral assay

- Electroconvulsive stimulation (ECS) paradigm
- Immunofluorescence
- Image acquisition and analysis
- Quantitative real time PCR
- *In vitro* protein expression
- Co-immunoprecipitation and Western Blot

- QUANTIFICATION AND STATISTICAL ANALYSIS
  - Quantification of immunofluorescent images
- STATISTICAL ANALYSIS

SUPPLEMENTAL INFORMATION

Supplemental information can be found online at https://doi.org/10.1016/j.isci.2022.105731.

ACKNOWLEDGMENTS

We thank Drs. T. Uemura, F-B. Gao, and J-Q. Ni, as well as the Bloomington *Drosophila* Stock Center and TsingHua Fly Center for providing fly strains. We thank Dr. J.D. Axelrod for providing the Pk antibody and Dr. H. Aberle for the Ank2-XL antibody. We thank Dr. L. Liu for supporting the establishment of the ECS paradigm. We thank Dr. T. Juelich (UCAS, Beijing) for linguistic assistance during the preparation of our manuscript. This study was supported by the National Key R&D Program of China (2019YFA0802402), the National Natural Science Foundation of China (Grants 31730045 and 31970947), Shenzhen-Hong Kong Institute of Brain Science-Shenzhen Fundamental Research Institutions (NYKFKT2019011), Key Research Program of Frontier Sciences-CAS (QYZDYSSW-SMC015), and the Chinese Academy of Sciences Interdisciplinary Innovation Team.

AUTHOR CONTRIBUTIONS

Y.C., T-T.L. and Y.L. conceived the project and designed the experiments. Y.C., T-T.L., X.L., and T.L. performed morphological studies. Y.C. and M.N. conducted behavioral assay. T-T.L. and X.W. performed the ECM recording. T-T.L. and Y.C. conducted cell culture and co-IP experiments. Y.C., T-T.L., and Y.L. wrote the manuscript.

DECLARATION OF INTERESTS

The authors declare no competing interests.

Received: January 5, 2022
Revised: July 27, 2022
Accepted: December 1, 2022
Published: January 20, 2023

REFERENCES

1. Bassuk, A.G., Wallace, R.H., Buhr, A., Buller, A.R., Afawi, Z., Shimojo, M., Miyata, S., Chen, S., Gonzalez-Alegre, P., Griesbach, H.L., et al. (2008). A homozygous mutation in human PRICKLE1 causes an autosomal-recessive progressive myoclonus epilepsy-ataxia syndrome. Am. J. Hum. Genet. *83*, 572–581. https://doi.org/10.1016/j.ajhg.2008.10.003.

2. Mastrangelo, M., Tolve, M., Martinelli, M., Di Noia, S.P., Parrini, E., and Leuzzi, V. (2018). PRICKLE1-related early onset epileptic encephalopathy. Am. J. Med. Genet. *176*, 2841–2845. https://doi.org/10.1002/ajmg.a.40625.

3. Tao, H., Manak, J.R., Sowers, L., Mei, X., Kiyonari, H., Abe, T., Dahdaleh, N.S., Yang, T., Wu, S., Chen, S., et al. (2011). Mutations in prickle orthologs cause seizures in flies, mice, and humans. Am. J. Hum. Genet. *88*, 138–149. https://doi.org/10.1016/j.ajhg.2010.12.012.

4. Todd, B.P., and Bassuk, A.G. (2018). A de novo mutation in PRICKLE1 associated with myoclonic epilepsy and autism spectrum disorder. J. Neurogenet. *32*, 313–315. https://doi.org/10.1080/01677063.2018.1473862.

5. Algahtani, H., Al-Hakami, F., Al-Shehri, M., Shirah, B., Al-Qahtani, M.H., Abdulkareem, A.A., and Naseer, M.I. (2019). A very rare form of autosomal dominant progressive myoclonus epilepsy caused by a novel variant in the PRICKLE1 gene. Seizure *69*, 133–139. https://doi.org/10.1016/j.seizure.2019.04.016.

6. Ehaideb, S.N., Wignall, E.A., Kasuya, J., Evans, W.H., Iyengar, A., Koerselman, H.L., Lilienthal, A.J., Bassuk, A.G., Kitamoto, T., and Manak, J.R. (2016). Mutation of orthologous prickle genes causes a similar epilepsy syndrome in flies and humans. Ann. Clin. Transl. Neurol. *3*, 695–707. https://doi.org/10.1002/acn3.334.

7. Mei, X., Wu, S., Bassuk, A.G., and Slusarski, D.C. (2013). Mechanisms of prickle1a function in zebrafish epilepsy and retinal neurogenesis. Dis. Model. Mech. *6*, 679–688. https://doi.org/10.1242/dmm.010793.

8. Ehaideb, S.N., Iyengar, A., Ueda, A., Iacobucci, G.J., Cranston, C., Bassuk, A.G., Gubb, D., Axelrod, J.D., Gunawardena, S., Wu, C.F., and Manak, J.R. (2014). Prickle modulates microtubule polarity and axonal transport to ameliorate seizures in flies. Proc. Natl. Acad. Sci. USA *111*, 11187–11192. https://doi.org/10.1073/pnas.1403357111.

9. Ban, Y., Yu, T., Wang, J., Wang, X., Liu, C., Baker, C., and Zou, Y. (2022). Mutation of the

murine Prickle1 (R104Q) causes phenotypes analogous to human symptoms of epilepsy and autism. Exp. Neurol. *347*, 113880. https://doi.org/10.1016/j.expneurol.2021.113880.

10. Yang, Y., and Mlodzik, M. (2015). Wnt-frizzled/planar cell polarity signaling: cellular orientation by facing the wind (wnt). Annu. Rev. Cell Dev. Biol. *31*, 623–646. https://doi.org/10.1146/annurev-cellbio-100814-125315.

11. Gubb, D., Green, C., Huen, D., Coulson, D., Johnson, G., Tree, D., Collier, S., and Roote, J. (1999). The balance between isoforms of the Prickle LIM domain protein is critical for planar polarity in Drosophila imaginal discs. Genes Dev. *13*, 2315–2327. https://doi.org/10.1101/gad.13.17.2315.

12. Strutt, H., and Strutt, D. (2021). How do the Fat-Dachsous and core planar polarity pathways act together and independently to coordinate polarized cell behaviours? Open Biol. *11*, 200356. https://doi.org/10.1098/rsob.200356.

13. Paemka, L., Mahajan, V.B., Skeie, J.M., Sowers, L.P., Ehaideb, S.N., Gonzalez-Alegre, P., Sasaoka, T., Tao, H., Miyagi, A., Ueno, N., et al. (2013). PRICKLE1 interaction with SYNAPSIN I reveals a role in autism spectrum disorders. PLoS One *8*, e80737. https://doi.org/10.1371/journal.pone.0080737.

14. Sanchez-Alvarez, L., Visanuvimol, J., McEwan, A., Su, A., Imai, J.H., and Colavita, A. (2011). VANG-1 and PRKL-1 cooperate to negatively regulate neurite formation in Caenorhabditis elegans. PLoS Genet. *7*, e1002257. https://doi.org/10.1371/journal.pgen.1002257.

15. Ahsan, K., Singh, N., Rocha, M., Huang, C., and Prince, V.E. (2019). Prickle1 is required for EMT and migration of zebrafish cranial neural crest. Dev. Biol. *448*, 16–35. https://doi.org/10.1016/j.ydbio.2019.01.018.

16. Yang, T., Kersigo, J., Wu, S., Fritzsch, B., and Bassuk, A.G. (2017). Prickle1 regulates neurite outgrowth of apical spiral ganglion neurons but not hair cell polarity in the murine cochlea. PLoS One *12*, e0183773. https://doi.org/10.1371/journal.pone.0183773.

17. Ban, Y., Yu, T., Feng, B., Lorenz, C., Wang, X., Baker, C., and Zou, Y. (2021). Prickle promotes the formation and maintenance of glutamatergic synapses by stabilizing the intercellular planar cell polarity complex. Sci. Adv. *7*, eabh2974. https://doi.org/10.1126/sciadv.abh2974.

18. Liu, C., Lin, C., Whitaker, D.T., Bakeri, H., Bulgakov, O.V., Liu, P., Lei, J., Dong, L., Li, T., and Swaroop, A. (2013). Prickle1 is expressed in distinct cell populations of the central nervous system and contributes to neuronal morphogenesis. Hum. Mol. Genet. *22*, 2234–2246. https://doi.org/10.1093/hmg/ddt075.

19. Allen, N.J., and Lyons, D.A. (2018). Glia as architects of central nervous system formation and function. Science *362*, 181–185. https://doi.org/10.1126/science.aat0473.

20. Henkel, J.S., Beers, D.R., Zhao, W., and Appel, S.H. (2009). Microglia in ALS: the good, the bad, and the resting. J. Neuroimmune Pharmacol. *4*, 389–398. https://doi.org/10.1007/s11481-009-9171-5.

21. Reindl, M., and Waters, P. (2019). Myelin oligodendrocyte glycoprotein antibodies in neurological disease. Nat. Rev. Neurol. *15*, 89–102. https://doi.org/10.1038/s41582-018-0112-x.

22. de Curtis, M., Garbelli, R., and Uva, L. (2021). A hypothesis for the role of axon demyelination in seizure generation. Epilepsia *62*, 583–595. https://doi.org/10.1111/epi.16824.

23. Di Nunzio, M., Di Sapia, R., Sorrentino, D., Kebede, V., Cerovic, M., Gullotta, G.S., Bacigaluppi, M., Audinat, E., Marchi, N., Ravizza, T., and Vezzani, A. (2021). Microglia proliferation plays distinct roles in acquired epilepsy depending on disease stages. Epilepsia *62*, 1931–1945. https://doi.org/10.1111/epi.16956.

24. Hiragi, T., Ikegaya, Y., and Koyama, R. (2018). Microglia after seizures and in epilepsy. Cells *7*, 26. https://doi.org/10.3390/cells7040026.

25. Wetherington, J., Serrano, G., and Dingledine, R. (2008). Astrocytes in the epileptic brain. Neuron *58*, 168–178. https://doi.org/10.1016/j.neuron.2008.04.002.

26. Devinsky, O., Vezzani, A., Najjar, S., De Lanerolle, N.C., and Rogawski, M.A. (2013). Glia and epilepsy: excitability and inflammation. Trends Neurosci. *36*, 174–184. https://doi.org/10.1016/j.tins.2012.11.008.

27. Misawa, S., Kuwabara, S., Hirano, S., Shibuya, K., Arai, K., and Hattori, T. (2004). Epilepsia partialis continua as an isolated manifestation of motor cortical dysplasia. J. Neurol. Sci. *225*, 157–160. https://doi.org/10.1016/j.jns.2004.07.014.

28. Wibom, R., Lasorsa, F.M., Töhönen, V., Barbaro, M., Sterky, F.H., Kucinski, T., Naess, K., Jonsson, M., Pierri, C.L., Palmieri, F., and Wedell, A. (2009). AGC1 deficiency associated with global cerebral hypomyelination. N. Engl. J. Med. *361*, 489–495. https://doi.org/10.1056/Nejmoa0900591.

29. Kelley, B.J., and Rodriguez, M. (2009). Seizures in patients with multiple sclerosis epidemiology, pathophysiology and management. CNS Drugs *23*, 805–815. https://doi.org/10.2165/11310900-000000000-00000.

30. Gibson, E.M., Geraghty, A.C., and Monje, M. (2018). Bad wrap: myelin and myelin plasticity in health and disease. Dev. Neurobiol. *78*, 123–135. https://doi.org/10.1002/dneu.22541.

31. Sugimura, K., Yamamoto, M., Niwa, R., Satoh, D., Goto, S., Taniguchi, M., Hayashi, S., and Uemura, T. (2003). Distinct developmental modes and lesion-induced reactions of dendrites of two classes of Drosophila sensory neurons. J. Neurosci. *23*, 3752–3760.

32. Pavlidis, P., and Tanouye, M.A. (1995). Seizures and failures in the giant fiber pathway of Drosophila bang-sensitive paralytic mutants. J. Neurosci. *15*, 5810–5819.

33. Kremer, M.C., Jung, C., Batelli, S., Rubin, G.M., and Gaul, U. (2017). The glia of the adult Drosophila nervous system. Glia *65*, 606–638. https://doi.org/10.1002/glia.23115.

34. Ng, J. (2012). Wnt/PCP proteins regulate stereotyped axon branch extension in Drosophila. Development *139*, 165–177. https://doi.org/10.1242/dev.068668.

35. Saras, A., Wu, V.V., Brawer, H.J., and Tanouye, M.A. (2017). Investigation of seizure-susceptibility in a Drosophila melanogaster model of human epilepsy with optogenetic stimulation. Genetics *206*, 1739–1746. https://doi.org/10.1534/genetics.116.194779.

36. Hekmat-Scafe, D.S., Mercado, A., Fajilan, A.A., Lee, A.W., Hsu, R., Mount, D.B., and Tanouye, M.A. (2010). Seizure sensitivity is ameliorated by targeted expression of K+-Cl- cotransporter function in the mushroom body of the Drosophila brain. Genetics *184*, 171–183. https://doi.org/10.1534/genetics.109.109074.

37. Yamamoto, M., Ueda, R., Takahashi, K., Saigo, K., and Uemura, T. (2006). Control of axonal sprouting and dendrite branching by the Nrg-Ank complex at the neuron-glia interface. Curr. Biol. *16*, 1678–1683. https://doi.org/10.1016/j.cub.2006.06.061.

38. Silies, M., and Klämbt, C. (2010). APC/C(Fzr/Cdh1)-dependent regulation of cell adhesion controls glial migration in the Drosophila PNS. Nat. Neurosci. *13*, 1357–1364. https://doi.org/10.1038/nn.2656.

39. Dzhashiashvili, Y., Zhang, Y., Galinska, J., Lam, I., Grumet, M., and Salzer, J.L. (2007). Nodes of Ranvier and axon initial segments are ankyrin G-dependent domains that assemble by distinct mechanisms. J. Cell Biol. *177*, 857–870. https://doi.org/10.1083/jcb.200612012.

40. Feinberg, K., Eshed-Eisenbach, Y., Frechter, S., Amor, V., Salomon, D., Sabanay, H., Dupree, J.L., Grumet, M., Brophy, P.J., Shrager, P., and Peles, E. (2010). A glial signal consisting of gliomedin and NrCAM clusters axonal Na+ channels during the formation of nodes of Ranvier. Neuron *65*, 490–502. https://doi.org/10.1016/j.neuron.2010.02.004.

41. Enneking, E.M., Kudumala, S.R., Moreno, E., Stephan, R., Boerner, J., Godenschwege, T.A., and Pielage, J. (2013). Transsynaptic coordination of synaptic growth, function, and stability by the L1-type CAM neuroglian. PLoS Biol. *11*, e1001537. https://doi.org/10.1371/journal.pbio.1001537.

42. Jegla, T., Nguyen, M.M., Feng, C., Goetschius, D.J., Luna, E., van Rossum, D.B., Kamel, B., Pisupati, A., Milner, E.S., and Rolls, M.M. (2016). Bilaterian giant ankyrins have a common evolutionary origin and play a conserved role in patterning the axon initial segment. PLoS Genet. *12*, e1006457. https://doi.org/10.1371/journal.pgen.1006457.

43. Zarin, A.A., Asadzadeh, J., Hokamp, K., McCartney, D., Yang, L., Bashaw, G.J., and Labrador, J.P. (2014). A transcription factor network coordinates attraction, repulsion,

and adhesion combinatorially to control motor axon pathway selection. Neuron *81*, 1297–1311. https://doi.org/10.1016/j.neuron.2014.01.038.

44. Stephan, R., Goellner, B., Moreno, E., Frank, C.A., Hugenschmidt, T., Genoud, C., Aberle, H., and Pielage, J. (2015). Hierarchical microtubule organization controls axon caliber and transport and determines synaptic structure and stability. Dev. Cell *33*, 5–21. https://doi.org/10.1016/j.devcel.2015.02.003.

45. Rasband, M.N., and Peles, E. (2021). Mechanisms of node of Ranvier assembly. Nat. Rev. Neurosci. *22*, 7–20. https://doi.org/10.1038/s41583-020-00406-8.

46. Chang, K.J., Zollinger, D.R., Susuki, K., Sherman, D.L., Makara, M.A., Brophy, P.J., Cooper, E.C., Bennett, V., Mohler, P.J., and Rasband, M.N. (2014). Glial ankyrins facilitate paranodal axoglial junction assembly. Nat. Neurosci. *17*, 1673–1681. https://doi.org/10.1038/nn.3858.

47. Otto, N., Marelja, Z., Schoofs, A., Kranenburg, H., Bittern, J., Yildirim, K., Berh, D., Bethke, M., Thomas, S., Rode, S., et al. (2018). The sulfite oxidase Shopper controls neuronal activity by regulating glutamate homeostasis in Drosophila ensheathing glia. Nat. Commun. *9*, 3514. https://doi.org/10.1038/s41467-018-05645-z.

48. Nave, K.A., and Werner, H.B. (2021). Ensheathment and myelination of axons: evolution of glial functions. Annu. Rev. Neurosci. *44*, 197–219. https://doi.org/10.1146/annurev-neuro-100120-122621.

49. Poser, C.M., and Brinar, V.V. (2003). Epilepsy and multiple sclerosis. Epilepsy Behav. *4*, 6–12. https://doi.org/10.1016/S1525-5050(02)00646-7.

50. Calabrese, M., Castellaro, M., Bertoldo, A., De Luca, A., Pizzini, F.B., Ricciardi, G.K., Pitteri, M., Zimatore, S., Magliozzi, R., Benedetti, M.D., et al. (2017). Epilepsy in multiple sclerosis: the role of temporal lobe damage. Mult. Scler. *23*, 473–482. https://doi.org/10.1177/1352458516651502.

51. Siegenthaler, D., Enneking, E.M., Moreno, E., and Pielage, J. (2015). L1CAM/Neuroglian controls the axon-axon interactions establishing layered and lobular mushroom body architecture. J. Cell Biol. *208*, 1003–1018. https://doi.org/10.1083/jcb.201407131.

52. Cammarota, C., Finegan, T.M., Wilson, T.J., Yang, S., and Bergstralh, D.T. (2020). An axon-pathfinding mechanism preserves epithelial tissue integrity. Curr. Biol. *30*, 5049–5057.e3. https://doi.org/10.1016/j.cub.2020.09.061.

53. Fréal, A., Rai, D., Tas, R.P., Pan, X., Katrukha, E.A., van de Willige, D., Stucchi, R., Aher, A., Yang, C., Altelaar, A.F.M., et al. (2019). Feedback-driven assembly of the axon initial segment. Neuron *104*, 305–321.e8. https://doi.org/10.1016/j.neuron.2019.07.029.

54. Jenkins, P.M., Kim, N., Jones, S.L., Tseng, W.C., Svitkina, T.M., Yin, H.H., and Bennett, V. (2015). Giant ankyrin-G: a critical innovation in vertebrate evolution of fast and integrated neuronal signaling. Proc. Natl. Acad. Sci. USA *112*, 957–964. https://doi.org/10.1073/pnas.1416544112.

55. Hebbar, M., and Mefford, H.C. (2020). Recent advances in epilepsy genomics and genetic testing. F1000Res. *9*. https://doi.org/10.12688/f1000research.21366.1.

56. Barry, J., Gu, Y., Jukkola, P., O'Neill, B., Gu, H., Mohler, P.J., Rajamani, K.T., and Gu, C. (2014). Ankyrin-G directly binds to kinesin-1 to transport voltage-gated Na+ channels into axons. Dev. Cell *28*, 117–131. https://doi.org/10.1016/j.devcel.2013.11.023.

57. Olofsson, J., Sharp, K.A., Matis, M., Cho, B., and Axelrod, J.D. (2014). Prickle/spiny-legs isoforms control the polarity of the apical microtubule network in planar cell polarity. Development *141*, 2866–2874. https://doi.org/10.1242/dev.105932.

58. Kuebler, D., and Tanouye, M.A. (2000). Modifications of seizure susceptibility in Drosophila. J. Neurophysiol. *83*, 998–1009. https://doi.org/10.1152/jn.2000.83.2.998.

59. Koch, I., Schwarz, H., Beuchle, D., Goellner, B., Langegger, M., and Aberle, H. (2008). Drosophila ankyrin 2 is required for synaptic stability. Neuron *58*, 210–222. https://doi.org/10.1016/j.neuron.2008.03.019.

60. Schindelin, J., Arganda-Carreras, I., Frise, E., Kaynig, V., Longair, M., Pietzsch, T., Preibisch, S., Rueden, C., Saalfeld, S., Schmid, B., et al. (2012). Fiji: an open-source platform for biological-image analysis. Nat. Methods *9*, 676–682. https://doi.org/10.1038/nmeth.2019.

61. Meijering, E., Jacob, M., Sarria, J.C.F., Steiner, P., Hirling, H., and Unser, M. (2004). Design and validation of a tool for neurite tracing and analysis in fluorescence microscopy images. Cytometry A. *58*, 167–176. https://doi.org/10.1002/cyto.a.20022.

STAR★METHODS

KEY RESOURCES TABLE

REAGENT or RESOURCE	SOURCE	IDENTIFIER
Antibodies		
Mouse anti-Bruchpilot	DSHB	nc82; AB_2314866
Mouse anti-Repo	DSHB	8D12; AB_528448
Mouse anti-Neuroglian	DSHB	BP 104;AB_528402
Mouse anti-Fasciclin II	DSHB	1D4; AB_528235
Rabbit anti-Ank2-XL	gift from H. Aberle	N/A
Guinea pig anti-Pk	gift from J. D. Axelrod	N/A
Goat anti-HRP DyLight 405	Jackson ImmunoResearch Labs	123-475-021
Goat anti-mouse IgG Alexa Fluor 488	Thermo Fisher	A-11029; AB_2534088
Goat anti-mouse IgG Alexa Fluor 555	Thermo Fisher	A-21424; AB_141780
Goat anti-rabbit IgG Alexa Fluor 555	Thermo Fisher	A-21429; AB_2535850
Goat anti-rabbit IgG Alexa Fluor 633	Thermo Fisher	A-21071; AB_2535732
Goat anti-Guinea Pig IgG Alexa Fluor 555	Thermo Fisher	A-21435; AB_2535856
Anti-HA epitope Agarose conjugate (2-2.2.14)	Santa Cruz	sc-500777A
Mouse anti-HA epitope	ABclonal	AE008; AB_2770404
Mouse anti-Flag epitope	ABclonal	AE005; AB_2770401
Mouse anti-Myc epitope	ABclonal	AE010; AB_2770408
Mouse anti-V5 epitope	ABclonal	AE017; AB_2770413
Mouse anti-β-Tubulin	ABclonal	AC021; AB_2773004
Mouse anti-GAPDH	ABclonal	AC002; AB_2736879
Goat Anti-Rabbit IgG HRP	CWBIO	CW0103S
Goat Anti-Mouse IgG HRP	CWBIO	CW0102S
Chemicals, peptides, and recombinant proteins		
Vectashield	Vector Laboratories	H-1000
Protein G PLUS-Agarose	Santa Cruz	sc-2002
TGX™ FastCast™ Acrylamide Kit, 10%	Bio-Rad	1610173
TGX™ FastCast™ Acrylamide Kit, 12%	Bio-Rad	1610175
Paraformaldehyde Aqueous Solution, 8%	EMS	157-8
DMEM, high glucose, GlutaMAX	Gibco	10566-016
Trypsin-EDTA (0.25%), phenol red	Gibco	25200-056
Goat Serum	Gibco	16210-072
Foetal Bovine Serum	Biological Industries	04-001-1ACS
TRIzol Reagent	Thermo Fisher	15596-018
PrimeScript™ RT reagent Kit with gDNA Eraser	Takara	RR047A
Lipofectamine™ 3000 Transfection Reagent	Thermo Fisher	L3000-015
Schneider's *Drosophila* Medium	GIBCO	21720-024
Critical commercial assays		
TB Green® Premix Ex Taq™ II (Tli RNaseH Plus)	Takara	RR820A
ECL Basic Plus Kit	ABclonal	RM00020P

(*Continued on next page*)

Continued

REAGENT or RESOURCE	SOURCE	IDENTIFIER
Experimental models: Organisms/strains		
Drosophila: *pk*$^{IG1-1}$	gift from T. Uemura	N/A
Drosophila: *pk*^{1}	KYOTO Stock Center	105875
Drosophila: *sple*^{1}	Bloomington Drosophila Stock Center	422
Drosophila: *nrg*^{17}	Bloomington Drosophila Stock Center	5595
Drosophila: *ank2*^{M}	Bloomington Drosophila Stock Center	24715
Drosophila: *ank2*^{f00518}	Bloomington Drosophila Stock Center	85608
Drosophila: *pk*$^{MI07065-TG4.2}$/SM6a	Bloomington Drosophila Stock Center	66864
Drosophila: UAS-mCD4-GFP	Bloomington Drosophila Stock Center	5137
Drosophila: UAS-RFP	Bloomington Drosophila Stock Center	7118
Drosophila: UAS-Pk	Bloomington Drosophila Stock Center	41777
Drosophila: UAS-Sple	Bloomington Drosophila Stock Center	41780
Drosophila: UAS-Nrg180	Bloomington Drosophila Stock Center	24169
Drosophila: R85G01-Gal4	Bloomington Drosophila Stock Center	40436
Drosophila: R56F03-Gal4	Bloomington Drosophila Stock Center	39157
Drosophila: R75H03-Gal4	Bloomington Drosophila Stock Center	39908
Drosophila: R55B03-Gal4	Bloomington Drosophila Stock Center	39101
Drosophila: R86E01-Gal4	Bloomington Drosophila Stock Center	45914
Drosophila: R54C07-Gal4	Bloomington Drosophila Stock Center	50472
Drosophila: R54H02-Gal4	Bloomington Drosophila Stock Center	45784
Drosophila: R56F03-LexA	Bloomington Drosophila Stock Center	53574
Drosophila: *repo*-Gal4	Bloomington Drosophila Stock Center	7415
Drosophila: R27E08-lexA	Bloomington Drosophila Stock Center	52676
Drosophila: repo-LexA	Bloomington Drosophila Stock Center	67096
Drosophila: UAS-Fas2.YFP	KYOTO Stock Center	116986
Drosophila: UAS-*pk*-RNAi	Tsinghua Fly Center	0859
Drosophila: UAS-*nrg*-RNAi	Tsinghua Fly Center	THU3730
Drosophila: UAS-*ank2*-RNAi	Tsinghua Fly Center	THU3560
Drosophila: *pk*^{325}	This paper	N/A
Oligonucleotides		
Primers for cloning, see Table S1	This paper	N/A
Primer for qPCR: *pk*-exon1-5-F (AGACATCAGCCCGTAGAACG)	This paper	N/A
Primer for qPCR: *pk*-exon1-5-R (GATGGGCCTTTCTAGCTCAA)	This paper	N/A
Primer for qPCR: *pk*-qpcr-2-F (GTGAGTGCCAATCAAGCGAC)	This paper	N/A
Primer for qPCR: *pk*-qpcr-2-R (TTAGCGGAGTTCGGCTGATG)	This paper	N/A
Primer for qPCR: *sple*-exon4-5-F (TGCCCACGATATCAGTTTCA)	This paper	N/A
Primer for qPCR: *sple*-exon4-5-R (GCTGATGGGCTCATTTGACT)	This paper	N/A
Primer for qPCR: *rp49*-RT-F (AGGGTATCGACAACAGAGTG)	This paper	N/A
Primer for qPCR: *rp49*-RT-R (CACCAGGAACTTCTTGAATC)	This paper	N/A
Software and algorithms		
GraphPad Prism	GraphPad Software	RRID: SCR_002798
ImageJ	National Institutes of Health (NIH)	RRID: SCR_002285
MATLAB	MathWorks	RRID:SCR_001622
NIS-Elements	Nikon	RRID:SCR_014329

RESOURCE AVAILABILITY

Lead contact

Further information and requests for resources and reagents should be directed to and will be fulfilled by the lead contact, Yan Li (liyan@ibp.ac.cn).

Materials availability

Fly lines and plasmids generated in this study are available on request.

Data and code availability

All data reported in this paper will be available from the lead contact upon request.

This paper does not report original code.

Any additional information required to reanalyze the data reported in this paper is available from the lead contact upon request.

EXPERIMENTAL MODEL AND SUBJECT DETAILS

Fly strains and constructs

Flies were maintained at 25°C with 12/12 light/dark cycles. Adult female flies aged between 6 and 7 days were used for behavioral and imaging experiments. For immunofluorescent experiments using larvae, the larvae were picked randomly without any preference for sex. $pk^{IG1\text{-}1}$ was a gift from Dr. Tadashi Uemura (Kyoto University). pk^{1} (105875) and UAS-Fas2.YFP (116986) were purchased from KYOTO Stock Center (DGRC). UAS-*pk*-RNAi, UAS-*nrg*-RNAi and UAS-*ank2*-RNAi were provided by Dr. Jian-Quan Ni (Tsinghua Fly Center, School of Medicine, Tsinghua University). Mutant and UAS alleles, $sple^{1}$ (422), nrg^{17}(5595), $ank2^{M}$ (24715), $ank2^{f00518}$ (85608), UAS-mCD4-GFP (5137), UAS-mRFP (7118), UAS-Pk (41777), UAS-Sple (41780), UAS-Nrg180 (24169), and $pk^{MI07065\text{-}TG4.2}$/SM6a (66864), were obtained from Bloomington Stock Center. A set of glia-expressing fly strains, R85G01-Gal4 (40436, PNG), R56F03-Gal4 (39157, EGN), R75H03-Gal4 (39908, EGT), R55B03-Gal4 (39101, L-ALG), R86E01-Gal4 (45914, ALG), R54C07-Gal4 (50472, SPG), R54H02-Gal4 (45784, CG), R56F03-LexA (53574, EGN) and *repo*-Gal4 (7415, pan-glia) were also obtained from Bloomington Stock Center.

To generate transgenic flies, UAS-V5-Ank2-com plasmid was constructed by cloning the DNA fragment encoding 1–1126 amino acids of Ank2 into an N-V5 tagged pUAST vector. LexAop-Pk and LexAop-Sple plasmids were constructed by cloning the cDNA encoding Pk and Sple into the pJFRC19 vector (Addgene). The sequence of primers used to generate transgenic flies and plasmids for cell transfection are listed in Table S1.

To remove the Gal4 element, $pk^{IG1\text{-}1}$mutant flies were subjected to delta2-3 transposase-induced hop-out experiments. A strain recovered with imprecise excision, leaving 325 bp of the P-element remaining at the insertion site, thus termed pk^{325}.

METHOD DETAILS

Behavioral assay

High-magnification videos of single flies were recorded to analyze spontaneous seizures.[6] Female flies were shortly cold-anesthetized on ice, then individually placed in an arena of 1.5-cm diameter. The flies were allowed to recover for 5 minutes and subjected to video recording. The videos were taken by an ANDOR Zyla sCMOS camera equipped on a Nikon SMZ25 dissection scope. A seizure event was defined as being incapable of keeping static, with convulsive leaping, rolling or paralysis lasting for at least one second. To assess the incidence of unprovoked seizures, flies were loaded individually into a 24-well plate, which was placed on an LED light panel. Videos were taken with a digital camera, and then analyzed by visual inspection. During a 5-minutes observation, flies with spontaneous seizures lasting for at least one second were counted.

A modified bang-sensitive assay was used to assess the provoked seizures of flies. Female flies were divided randomly into groups of 10 and aged 5–6 days before the test. On the day of the test, each group

of flies were transferred into a clean empty vial, where they were allowed to rest for 10 min. The vials were then vortexed for 30 s, immediately followed by video-taping for 30 s. Climbing off the bottom and staying on the wall was considered as recovery of voluntary movement. The number of flies recovered were scored every 5 s in a double-blind manner. The normalized difference of recovery rate (RR) was calculated as: $normalized\ difference\ of\ RR = \frac{RR - \overline{RR}_{control}}{\overline{RR}_{control}}$. The rescuing effect were defined as the difference of recovery rate between the rescue group and the mean recovery rate of the corresponding LexA and LexAop controls: $rescue\ effect = RR - \frac{\overline{RR}_{LexA} + \overline{RR}_{LexAop}}{2}$.

Electroconvulsive stimulation (ECS) paradigm

ECS paradigm was performed as previously described.[58] Female flies aged 6–7 days were anesthetized on ice, and attached to a tungsten pin using UV-curing glue, then allowed to rest 30 min before experiments. The spiking activities of the dorsal longitudinal flight muscle (DLM) were recorded by inserting a glass electrode through a small cut on the dorsal thorax, and a platinum reference electrode inserted between the thorax and abdomen. A pair of tungsten electrodes were pieced in the compound eyes to deliver ECS. The stimulus consists of a train of 0.1 ms pulses at 200 Hz lasting 2 s. For each fly, ECS of 0.1, 0.5 and 1.0 mA were delivered successively with 10-min intervals.

Immunofluorescence

To analyze neurite outgrowth and glial wrapping, we expressed mGFP using a pan-glial driver, *repo*-Gal4 or *repo*-LexA, to label glia. The ddaE neurons were labeled by either staining for a neuronal marker, HRP, or by $Gal4^{IG1\text{-}1}$>RFP. Wandering larvae at late 3^{rd} instar stage were dissected and immunostained according to standard protocols. Adult brain dissection and immunostaining was performed following the FlyLight protocols (Janelia Research Campus, HHMI). Larval preparations and adult brains were mounted using anti-fading mounting media (VECTASHIELD®, Vector Laboratories).

Mouse monoclonal antibodies against Nrg180 (BP104, 1:200) were purchased from Developmental Studies Hybridoma Bank (DSHB, University of Iowa). Dylight 405 conjugated anti-HRP (123-475-021, 1:500) was obtained from Jackson Immunoresearch Laboratories. Rabbit anti-Ank2XL was gifted by Dr. Hermann Aberle (Max-Plank Institute for Developmental Biology).[59] Guinea pig anti-Pk was gifted by Dr. Jeffrey D. Axelrod (Stanford University).[57] Secondary antibodies were Alexa Fluor® 555 Goat anti-mouse IgG (Invitrogen A21422, 1:500), Alexa Fluor® 633 Goat anti-rabbit IgG (Invitrogen A21070, 1:500), Alexa Fluor® 555 Goat anti-Guinea pig IgG (Invitrogen A21435, 1:500). Nuclei were stained with DAPI (Sigma-Aldrich, 28718-90-3).

Image acquisition and analysis

Immuno-stained samples were imaged using a Nikon A1 confocal microscope. For each staining, the imaging parameters were maintained identical for all samples. Images were processed and analyzed using the NIS-Element D 3.0 (Nikon) and Fiji software.[60]

To obtain *in vivo* imaging, wondering stage larvae were rinsed in PBS and immersed in a drop of 90% glycerol on a glass slide. A cover slip was used to immobilize the larvae with its dorsal side up. Images were acquired using a Leica SPE confocal microscope.

To analyze the peripheral glial wrapping, ddaE neurons were imaged in the A4-A6 segments of a larvae, and at least fifteen larvae were examined for each experimental group. Normal glial wrapping referred to cases where the entire cell body is enveloped by glial sheath. In contrast, defective glial wrapping was defined as the cases where part of or the entire cell body is stripped of glial sheath. The percentage of neurons with defective glial wrapping was compared using Fisher's exact test.

Quantitative real time PCR

20 larvae (68–70hr AEL), 20 pupae (15hr APF), or 10 adults were collected for total RNA extraction. Next, 1 μg of total RNA was reverse-transcribed using PrimeScript RT Master Mix (TaKaRa, RR047). Realtime quantitative PCR was carried out using a TB Green Premix Ex Taq II (Takara, RR820) and an ABI PRISM 7500 Realtime-PCR Detection system (Applied Biosystems). Relative mRNA levels were calculated using the comparative CT method. Gene *rp49* was used as an internal control, and gene expression levels

were normalized to *pk* levels of w^{1118} embryo or adult. Three independent repeats were performed. The following primers were used: *pk*-exon1-5-F (AGACATCAGCCCGTAGAACG), *pk*-exon1-5-R (GATGGGCC TTTCTAGCTCAA), *pk*-qpcr-2-F (GTGAGTGCCAATCAAGCGAC), *pk*-qpcr-2-R (TTAGCGGAGTTCGGCT GATG), *sple*-exon4-5-F (TGCCCACGATATCAGTTTCA); *sple*-exon4-5-R (GCTGATGGGCTCATTTGACT), *rp49*-RT-F (AGGGTATCGACAACAGAGTG), and *rp49*-RT-R (CACCAGGAACTTCTTGAATC).

In vitro protein expression

The full-length Pk, Sple and Nrg180 were PCR amplified from w^{1118} pupal cDNA with different tags attached to their N-terminal, and inserted into the NotI-XbaI sites of pcDNA3.1 vector (Invitrogen). To construct the HA-tagged common Pk fragment (HA-Pk-com), a DNA fragment encoding 14–963 amino acids of Pk was amplified by PCR from the HA-Pk construct, before being introduced into the NotI-XbaI sites of the pcDNA3.1 vector. HA-Pk-com-ΔPET and HA-Pk-com-ΔLIM were generated using PCR-driven overlap extension.

To construct the V5-tagged Ank2 common exon fragment (V5-Ank2-com), a DNA fragment encoding 1–1126 amino acids of Ank2 was amplified by PCR, and then cloned into the pcDNA3.1 vector through the EcoRI-XbaI sites. V5-Ank2-com-ΔSpec and V5-Ank2-com-ΔAnk were generated using PCR-driven overlap extension.

HEK293T cells were cultured in DMEM (Dulbecco's modified eagle medium; Gibco, 10566016) supplemented with 10% FBS (fetal bovine serum, Biological Industries, 04-001-1ACS) and 1% penicillin-streptomycin (Gibco, 15070063). Cells were transfected using Lipofectamin 3000 (Thermo Fisher, L3000-015) at least 20–24 h after plating.

Co-immunoprecipitation and Western Blot

For co-immunoprecipitation, cells were lysed 24 h after transfection with NP40 lysis buffer for 1 h on ice, and then centrifuged at 13,000g for 15minat 4°C. Antibody-coated agarose beads (Santa Cruz, 2-2.2.14) were added into the cell lysates and incubated overnight at 4°C. After being washed five times with lysis buffer, the beads were boiled in 40–60 μL of 1× reduced loading buffer at 100 °C for 8 min. The samples were resolved by SDS-PAGE, transferred to PVDF membrane and probed with HA (ABclonal, AE008), V5 (ABclonal, AE017), Myc (ABclonal, AE009) or Nrg180 antibody.

QUANTIFICATION AND STATISTICAL ANALYSIS

Quantification of immunofluorescent images

Image quantification was performed with Fiji software. To quantify immunofluorescent signals in ddaE neurons, cell body and neurites were manually outlined and traced, and the protein distribution was determined using the NeuronJ plugin.[61] To quantify immunofluorescent signals in the MB, signals of MBDsRed were median-filtered and converted to binary images with the threshold set by the Otsu method. The binary image stacks were used to measure the sectional area and the volume of MB subdivisions. The binary stacks of MBDsRed channel were also applied on other channels as masks to segregate the immunofluorescent signals within the MB. We developed a MATLAB script that performs virtual transverse sectioning along the longitudinal axis of the peduncle or the vertical lobe in 1 μm steps. Next, the area and the fluorescent intensity of each section were measured. The starting points of the vertical lobe and the peduncle were defined as the peduncle divide and the peduncle neck, respectively.

STATISTICAL ANALYSIS

Statistical analysis and data plotting were performed using Prism8 (GraphPad software). Student's *t*-test or Mann-Whitney test was used to compare the mean values of two experimental groups, and One-way ANOVA followed by corrected multiple comparison was used for comparing multiple groups. Two-way ANOVA followed by corrected multiple comparison was used to compare means among groups defined by two variables (e.g., genotype x time point). Incidence of spontaneous seizures and rate of defective glial wrapping were compared using the Fisher exact test. Results of statistical analysis are represented on the graphs as: *, $p< 0.05$; **, $p< 0.01$; ***, $p< 0.001$.